Influence of Preparation Method in the Electrochemical Performance of Lithium iron phosphate Cathodes

By

JAYALAKSHMI S

(Reg No. 21PPH004)

Supervisor

Dr. B. Nalini

Department of Physics

A Thesis submitted to

AVINASHILINGAM INSTITUTE FOR HOME SCIENCE AND HIGHER EDUCATION FOR WOMEN, COIMBATORE – 641 043.

In Partial Fulfilment of the requirements for the award of Degree

MASTER OF SCIENCE IN PHYSICS

MAY 2023

Influence of Preparation Method in the Electrochemical Performance of Lithium iron phosphate Cathodes

By

S. JAYALAKSHMI

(Reg No. 21PPH004)

Supervisor

Dr. B. Nalini

Department of Physics

A Thesis submitted to

AVINASHILINGAM INSTITUTE FOR HOME SCIENCE AND HIGHER EDUCATION FOR WOMEN, COIMBATORE – 641043

In partial Fulfillment of the Requirements of the Degree of

MASTER OF SCIENCE IN PHYSICS

MAY 2023

CERTIFIED AS A BONAFIDE RESEARCH WORK

12/05/23

Signature of Head of the Department

Dr. J. SHANTHI, M.Sc., M.Phil., Ph.D.,
Professor and Head
Department of Physics
Avinashilingam Institute for Home Science
and Higher Education For Women
Coimbatore - 641 043.

12/05/2023

Signature of the Supervisor

ACKNOWLEDGEMENT

We owe our sincere thanks to lord almighty, our reverent **founder Dr. T.S. Avinashilingam Ayya** and our **Amma Dr. Rajammal P. Devadas** and my lovable parents. Without whom we should have been nothing, for showering their generous blessing upon us in all endeavours.

I owe my sincere thanks to **lord almighty** and **my lovable parents** for showering their generous blessings upon me in all endeavours.

I wish to express my gratitude to **Prof. S.P. Thyagarajan** Ph.D, M.D., D.S, FAMS, FNASc,FIMSA,FABMS, FFTM (Glasgow, UK), Chancellor, Avinashilingam Institute for Home Science and higher education for women, Coimbatore, for providing the facilities to conduct this study.

I extend my thanks to **Dr. V. Bharathi Harishankar** Ph.D., FRSA, Vice Chancellor, Avinashilingam Institute for Home Science and higher education for women, Coimbatore, for providing flamboyant help towards the completion of the study.

I record my deep sense of gratitude and indebtedness to **Dr.(Mrs) S.Kowsalya** M.Sc., M.Phil,Ph.D Registrar, Avinashilingam Institute for Home Science and higher education for women, Coimbatore, for providing adequate help for the study.

I gratefully record my sincere thanks to **Dr.(Mrs.) G. Padmavathi** M.Sc., M.Phil., Ph.D., Dean, School of Physical Sciences and Computational Sciences, Avinashilingam Institute for Home Science and Higher Education for Women, Coimbatore, for timely help rendered throughout the course of this work

I whole heartily thank **Dr.(Mrs.) J. Shanthi,** M.Sc., M.Phil., Ph.D., Professor and Head, Department of Physics, Avinashilingam Institute for Home Science and Higher Education for Women, Coimbatore, for her encouragement and generous help which was of great value.

I express my heartiest thanks to my guide **Dr. (Mrs.) B. Nalini,** M.Sc., Ph.D., M.S (Edu.Mgt.), STA fellow, AIST Fellow (Japan), Assistant Professor, Avinashilingam Institute for Home Science and Higher Education for Women, University, Coimbatore, for her valuable guidance learned counsel, cordial treatment, keen interest, constant encouragement and care rendered throughout the course of my investigation.

I sincerely thank all **the staff members** of the Department of Physics, Avinashilingam Institute for Home Science and higher education for women, Coimbatore, for their help and support.

I would like to express my special thanks to **my parents, my friends** and all **my well-wishers** for their constant encouragement, support and help in carrying out this work

S. JAYALAKSHMI

CONTENT

LIST OF FIGURES

LIST OF TABLES

CHAPTER I

INTRODUCTION

Efficient and reliable energy storage systems are crucial for our modern society. Lithium-ion batteries (LIBs) with excellent performance are widely used in portable electronics and electric vehicles (EVs), but frequent fires and explosions limit their further and more widespread applications. Lithium-ion batteries (LIBs) have raised increasing interest due to their high potential for providing efficient energy storage and environmental sustainability [1]. LIBs are currently used not only in portable electronics, such as computers and cell phones, but also for electric or hybrid vehicles. In fact, for all those applications, LIBs' excellent performance and energy density have made them increasingly popular. In addition, the battery market for portable electronics is currently dominated by LIBs because of their inherent advantages over other battery systems, such as high specific capacity and voltage, no memory, excellent cycling performance, little self- discharge, and wide temperature range of operation [2]. Further expansion of the LIB market and its large-scale implications in EVs are at present significantly hindered. By their limited safety performance. In recent years, tons of LIBs have been recalled due to explosion and fire accidents [3], resulting in severe economic issues for related market sectors and significantly damaging the reputation of LIBs [4]. Consequently, increasing attention is being paid to LIB safety issues and a large number of safety strategies are being developed.

1.1 Energy storage device or Batteries:

Today, in developed nations, the supply and availability of energy are taken for granted. Lithium-battery technology over the past two decades by the discovery of new materials and designs through intuitive approaches, experimental and predictive reasoning, and meticulous control of surface structures and chemical reactions. Further improvements in energy density of factors of two to three may yet be achievable for current day lithium-ion systems; factors of five or more may be possible for lithium–oxygen systems, ultimately leading to our ability to confine extremely high potential energy in a small volume without compromising safety, but only if daunting technological barriers can be overcome. Lithium-ion batteries are one of the most popular forms of energy storage in the world. Li-ion batteries consist of lithium metal oxides in the positive electrode, and carbon in the negative electrode. The electrolyte used is lithium salts dissolved in organic carbonates. Lithium-ion batteries operate via the transfer of lithium ions in two phases. During charging, lithium ions pass from the positive to the negative

electrode, while the opposite occurs during discharging. Li-ion batteries do not require temperature monitoring to ensure effective operation. The large demand for Li-ion batteries is due to their accessibility and reliability.

The advantages of Li-ion batteries lead to their use in the production of large-scale storage systems, even if such storages will be expensive. Although Li-ion batteries have the highest price among all the battery-type energy storage devices, they offer the capability to store renewable energy because of their low cost per cycle. Lithium-ion batteries are extensively employed in a large variety of miniaturized electronic equipments. These types of batteries are mainly composed of a cathode immersed in an electrolyte solution separated by a selective membrane and a lithium-based anode. The performance of the lithium-ion batteries is always based on the conductivity of the electrodes. Lithium-ion batteries consisting of $LiCoO_2$ and graphite are popular worldwide as power sources for mobile phones, laptop computers, and other electronic devices. Graphite and $LiCoO_2$ are called lithium insertion materials. In other words, the lithium-ion battery consists of two lithium insertion materials. The combination of two lithium insertion materials is essential for the basic function of the lithium-ion battery [5].

1.2 Types of Batteries:

Battery is an energy storage device in which energy is stored in the form of chemical and they are classified as

i. Primary Battery
ii. Secondary Battery

1.2.1 Primary Battery:

Primary batteries, also called ‘disposable batteries’, still use the basic idea of a voltaic pile. Here the electrochemical energy produced by the decomposition of electrode material and electrolyte will break down once the electrode or the electrolyte are degraded. Since this procedure is irreversible, the battery needs to be replaced by a new battery. A primary battery is a battery in which the electrochemical reaction is not reversible. Primary batteries are typical power sources for sensor nodes. By supplying their energy at the required voltage levels, they eliminate the need for intermediate power conditioning electronics.

1.2.2 Secondary Battery:

Secondary (rechargeable) batteries can be recharged by applying a reverse current, as the electrochemical reaction is reversible. The original active materials at the two electrodes can be reconstituted chemically and structurally by the application of an electrical potential between the electrodes to "inject" energy. These batteries can be discharged and recharged many times. There are several types of secondary batteries that have been developed for mobile applications like cellular phones, power tools, and cars, where the potential in terms of specific power and specific energy appears to have reached a limit with today's most modern lithium-ion (Li-ion) batteries.

Rechargeable batteries power portable electronics, electric vehicles, and other electrical systems on demand by reversibly converting electrical and chemical potential energy through redox reactions at the interfaces between the electrodes and electrolyte [6].

1.3 Lithium Ion Battery (LIB):

The rechargeable lithium-ion battery is made of one or more power-generating compartments called cells. Each cell has essentially three components- positive electrode, negative electrode and electrolyte.

1.3.1 LIB working principle:

LIBs typically consist of four major parts: cathode, anode, separator, and electrolyte. Cathodes and anodes are the charge carriers contributing to LIB energy storage and release. The separator physically divides the electrodes to prevent internal short-circuits while allowing Li+ flow. The electrolyte carries ions, including Li+. The malfunction of these parts, together or individually, can negatively affect LIB safety. When operating, the electrodes produce heat, which might become uncontrollable during battery malfunction. If a separator is damaged, LIB processes transit from controlled to uncontrolled electrochemical reactions, with significant heat generation. In such cases, the electrolyte acts as a fuel supply for further heat generation, so appropriate safety regulations, which can be established by researching the controllable and uncontrollable factors in battery failures, are essential for improving LIB safety performance. The working mechanism of typical LIBs is shown in Fig. 1(a), using a $LiCoO_2$/graphite cell as an example. During charging, Li+ de-intercalates from the cathode materials ($LiCoO_2$, in this case), diffuses into the electrolyte and moves through the separator micro pores to intercalate into the anode material. Meanwhile, electrons move in the opposite direction through the

external circuit to maintain electro-neutrality. During discharging, Li+ ions transport from the anode side back to the cathode.

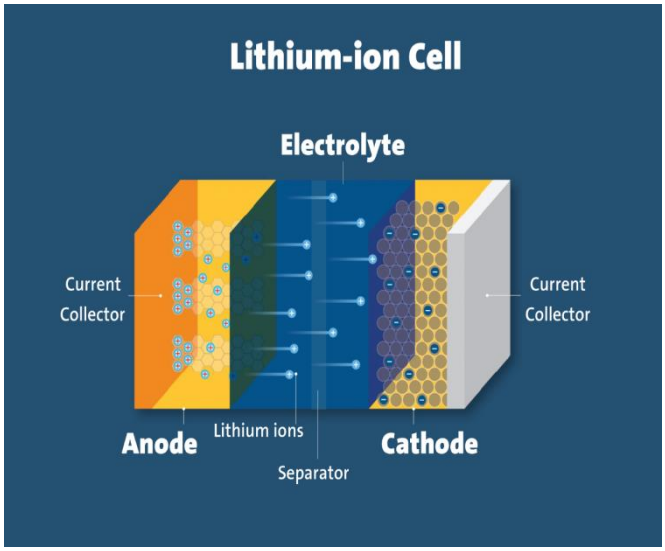

Figure 1. Working of Lithium Ion Battery

1.3.2 Positive Electrodes:

Since carbon (graphite) which is most commonly used as a negative electrode doesn't bear any Li-ions, the positive electrode must act as the source of Li. Thus, the cathodes are generally intercalation compounds from which Li+ ions can diffuse out or back in. High cathode voltage is generally desirable as energy stored in the cell is directly proportional to it. However, electrolyte stability also has to be considered. A number of candidates have been explored as suitable candidates for cathode materials of Li-ion batteries, and can be categorized based on voltage verses lithium.

1.3.3 Negative Electrodes:

Carbon anode has been dominant in the Li-ion battery industry since its commercialization as it renders excellent cyclability by facilitating the movement of lithium ions in and out of its lattice space with minimum irreversibility [5]. Carbons that are capable of reversible lithium-ion storage can be classified as graphitic and non-graphitic (dis-ordered) carbon. Graphitic carbons have a layered structure.

1.3.4 Electrolyte:

The electrolyte is the solution compromising the salts and the solvents and is the third component of the battery. The choice of electrolyte is very crucial and it determines the stability of the cell. The electrolyte is supposed to be chosen such that it can withstand the redox environment at both cathode and anode sides and the voltage range involved without decomposition or degradation.

1.3.5 Separator:

Optimizing the chemical stability of any electrode-electrolyte requires a control over the electrode-electrolyte interface through surface chemistry. Thus, separators are essential components of Li-ion batteries. The separator in a Li-ion battery plays the critical roles to avoid direct physical contact between the cathode and anode, and prevents short circuit to occur. At the same time, the separator allows lithium ions in the electrolyte to pass through it. The separators must be chemically stable and inert in contact with both electrolyte and electrodes [7].

1.4 Evolution of Lithium-ion battery:

Since lithium metal constituted a safety problem, attention got shifted to the use of a lithium-intercalation material as an anode. Ikeda of Sanyo was the first to patent an intercalation material in an organic solvent such as graphite in his June 1981 Japanese Patent No. 1769661. One year before the Ikeda patent on graphite, Goodenough filed his $LiCoO_2$ patent for an intercalation cathode material. Basu of Bell Laboratories filed U.S. Patent 4, 423, 125, in 1982, based on his finding of lithium intercalation in graphite at room temperature. Previously, Basu had found lithium intercalation into graphite in molten salt electrolytes at high temperatures (U.S. Patent 4,304,8259). Kuribayashi and Yoshino developed a new cell design using an intercalation carbon anode and a $LiCoO_2$ cathode and filed patents worldwide. Using a pilot plant developed for rechargeable Li-MnO_2 cells, Sony Energetic Inc. began to produce commercial cells (called the Li-Ion Battery) based on the Asahi patents in 1991. They also introduced electronic circuitry to control the charge-discharge, the use of a current interrupt device to interrupt current flow on build-up of excessive internal cell pressure, and the use of a "shut-down" polymer separator. The name "lithium-ion" now is accepted by the battery community worldwide, although there is no lithium metal in the cell. However, very often lithium-metal deposition occurs during charging with the graphite anode and it may cause

many troubles in the LIBs. Both electrodes operate by intercalation of lithium ions into the structure of the active materials. At Battery Co., a joint venture of Toshiba Battery Co. and Asahi Chemical Co., was the second to commercialize the technology using Asahi patent portfolio [8].

1.5 Recent development in lithium-ion battery technology:

1.5.1 Solid-State Batteries:

The most recent developments in lithium-ion battery technology have focused on improving the energy density and safety of the batteries. One of the biggest advancements in lithium-ion battery technology has been the development of solid-state batteries. Lithium-based solid-state batteries are projected to carry far more energy in the same volume and charge much faster than traditional Li-ion batteries. Instead of the liquid electrolytes used in conventional batteries, these batteries use solid-state electrolytes like ceramics or solid polymers. Smaller batteries with higher energy densities, longer life spans, and improved safety profiles may result from the application of this technology.

1.5.2 Nanotechnology:

Another crucial issue is battery safety. Li-ion batteries frequently use liquid electrolytes, which can overheat and cause the cell to rupture or even catch fire. Safety precautions are currently needed to prevent this, but they take up room inside the battery, increasing its size and the manufacturing process's cost and complexity.

Researchers working on nanotechnology are resolving these problems. Nanostructured materials can significantly increase the surface area for electrolyte materials, and nanoparticles may improve the conductivity of ceramics or gels to the point that they can substitute liquid electrolytes, lowering or eliminating the risk of a short circuit.

1.6 Availability of anodes for lithium-ion battery:

Anode materials for lithium batteries have been reviewed. Several elements of the group IV (C, Si, Ge and Sn) and group V (P, Sb) and their composites including Ag and Mg have been investigated. Agglomerated graphite NPs are currently used in newly developed LIBs. Replacement of conventional graphite microparticles by NPs will certainly increase charge/discharge (insertion/removal of Li^+) rates. However, when graphite NPs are used, catastrophic reactions may occur following lithium deposition and build-up. New anode

materials should allow higher redox potential along with high charge rate and low strain. Numerous anode perovskites like lithium titanates and alloys like (Li_xM_y) have been developed.

1.7 Availability of cathode for lithium-ion battery:

- **Lithium Cobalt Oxide (LCO)** – It is a cathode material composed of lithium, cobalt, and oxygen. On account of its low energy density, it is not often used for batteries in electric vehicles but is widely used in Li-ion batteries for portable electronics like smartphones. This chemistry gives good performance and is relatively safe, but due to the high cobalt content, it is also expensive and therefore, not used in EV applications.
- **Lithium Manganese Oxide (LMO)** – It is a cathode material composed of lithium, manganese, and oxygen. As it uses manganese it is inexpensive but at the same time is also vulnerable to high temperature. LMO batteries were used in the first EVs such as Nissan Leaf, on account of their high reliability and relatively low cost.
- **Lithium Nickel Manganese Oxide (NMC)** – It is a cathode material composed of lithium, nickel, manganese, cobalt, and oxygen. Simply put, it is LCO with nickel and manganese added. The proportion of cobalt within LCO was reduced to make room for nickel and cobalt. The proportion of nickel, cobalt, and manganese is usually 1:1:1 in NCM but recently R&D in progress are looking to increase nickel content for increased energy density while decreasing cobalt, which is expensive. Cathode material with more than 60 percent nickel is also called high nickel. It is a cathode material with high energy density due to the higher nickel proportion which creates strong and instantaneous energy.
- **Lithium Nickel Cobalt Oxide (NCO)** – It is a cathode material composed of lithium, nickel, cobalt, aluminium, and oxygen. It is an LCO with nickel and aluminium added. Usually nickel, cobalt, and aluminium are in 8:1:1 proportion. NCO cathode materials have a high proportion of nickel hence they are high in energy density have low stability. Therefore, they are used in smaller batteries rather than mid-to-large-sized batteries. Reports suggest that these were the first commercial attempts to substitute some of the expensive cobalt in the LCO cathode by increasing the nickel content [9].

- **Lithium Iron Phosphate (LFP)** – It is a cathode material composed of lithium, iron, phosphorous, and oxygen. Given that it uses iron, it is low-cost and safer than other cathode

chemistries, but LFP is also heavy and has lower energy capacity. They find use in passenger vehicles especially for shorter range and lower cost applications.

1.7.1 Lithium iron phosphate [LFP]:

$LiFePO_4$ is one of the most successfully commercialized cathode materials in rechargeable lithium-ion batteries (LIBs) system, owing to its excellent safety performance and remarkable electrochemical properties, which is expected to have a broader market in the near future. Therefore, demonstrating excellent safety features, $LiFePO_4$ has been the focus in both scientific research and industrial community since the first report in 1997 by Good enough et al. Moreover, its moderate operating voltage (3.5 V Li/Li+), moderate capacity (170 $mAhg^{-1}$), flat voltage plateau, abundant material supply, low material cost, and good environmental compatibility have also made $LiFePO_4$ a favourable cathode material for commercial LIBs. [10]

1.7.2 Structure of LFP:

The most stable polymorph of $LiFePO_4$ is olivine which has an orthorhombic structure with the space group of Pnma (a = 10.337 Å; b = 6.011 Å; c = 4.695 Å) [6]. As displayed in Fig.1, the lithium ions are situated at chains of edge-sharing octahedral, while the P^{5+} and Fe^{2+} ions are located at tetrahedral and octahedral sites respectively. The lithium ion in $LiFePO_4$ can be transferred from the cathode to the anode yielding the oxidation state from Fe^{2+} to Fe^{3+}.

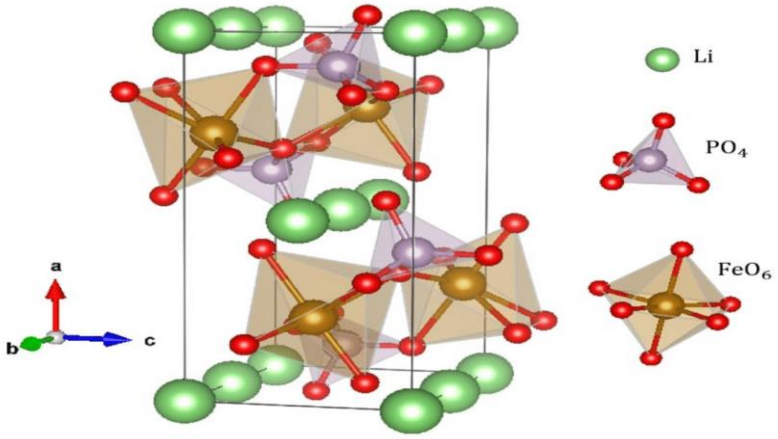

Figure 2. Structure of Lithium Iron Phosphate

1.8 Benefits of Lithium-ion Batteries:

Lithium-ion batteries are among the most popular rechargeable batteries in consumer electronics today. They offer many advantages over traditional batteries. Here are some of the key benefits of lithium-ion batteries:

- Longer Life: Lithium-ion batteries have a longer lifespan than traditional batteries, with some lasting up to 10 years or more. This makes them ideal for long-term use in laptops and smartphones.
- Higher Energy Density: Li-ion batteries can store more energy in a smaller space than other rechargeable batteries because they have a higher energy density. This makes them ideal for powering small, portable devices such as smartphones and tablets.
- Lower Self-Discharge Rate: These batteries have a lower self-discharge rate than other rechargeable batteries, meaning they retain their charge for longer periods. This makes them ideal for devices requiring long inactivity, such as medical equipment.
- Low Maintenance: They require little to no maintenance, making them ideal for devices used infrequently or stored for long periods [11].
- Environmentally Friendly: They are more environmentally friendly than other rechargeable batteries, as they contain fewer toxic materials and are easier to recycle.

1.9. Objective

- To evaluate the impact of synthesis procedure on LFP cathode for lithium-ion battery.
- To evaluate the electrochemical performance of the LFP cathode prepared by different methods.

1.10. Methodology

- To prepare lithium iron phosphate (LFP) by using sol gel method, solid state reaction method, hydrothermal method and co precipitation method.
- To characterize their structural and electrochemical properties.

CHAPTER II

REVIEW OF LITERATURE

Lithium-ion batteries provide their own unique advantages like high energy density, low maintenance, performance and longevity, and versatility. Lithium-iron phosphate is a good cathode material for Lithium-ion batteries. Phosphate compounds are promising materials for lithium-ion batteries because of their structural stability. The review of literature based on synthesis of Lithium iron phosphate are discussed. Four methods of preparation are chosen for preparing lithium iron phosphate. Review of literature for $LiFePO_4$ are discussed with the Li-starting materials, synthesis procedure and its electrochemical performance and listed in the Table 2.1.

Table. 2.1. Review of Literature based on $LiFePO_4$

Author & Year	**Material**	**Lithium starting material used**	**Methodology**	**Electrochemical Performance**	**Ref.**
Carlos A.G.Bezerra et.al.,(2021)	$LiFePO_4$	Li_3PO_4	Hydrothermal method	Specific capacity - 126mAhg^{-1} at 0.1C Columbic efficiency - 94 – 99%	**[12]**
Yin li, et.al., (2021)	$LiFePO_4$	$LiOH.H_2O$	Solvothermal method	Discharge capacity – 156.9 mAhg^{-1} ,150 cycles at 1C	**[13]**
Chaironilatif et.al., (2021)	$LiFePO_4$	Li_2CO_3	Dissolution method	Electrical conductivity - 3.25×10^{-5} Scm^{-1}	**[14]**
Yu-Xuan Bai(2020)	$LiFePO_4$/C/rGO	$LiOH.H_2O$	Sol-gel method and Spray-drying	Discharge capacity – 160.2 mAhg^{-1} at 0.1C	**[15]**
Wen-chenchein (2020)	$LiFePO_4$/C	LiH_2PO_4	Hydrothermal and Solid-phase method	Discharge specific capacity – 174.5 mAhg^{-1} at 0.1C for 5 cycles	**[16]**

Qianqian Li et.al., (2020)	$LiFePO_4$/ AC-P4	Li $_2CO_3$	In-situ plasma-assisted pyrolysis	Specific capacity – 166.9mAhg^{-1} at 0.2C	**[17]**
Xiaoning Tian et.al., (2020)	G/$LiFePO_4$/C	LiH_2PO_4	Micro reactor method	Specific capacity – 161.3 mAhg^{-1} at 0.2C	**[18]**
Bo Wang et.al.,(2020)	$LiFePO_4$/ rGO	LiOH	Co-precipitation technique	Reversible capacity – 158mAhg^{-1} at 0.1C and 1000 cycles at 10C.	**[19]**
Youngsuk, et.al.,(2019)	$LiFePO_4$/ rGO	LiOH.H2O	Spray coating method	Capacity -158 mAhg^{-1} at 0.1C	**[20]**
Ju-Won Jeoaet.al., (2019).	$LiFePO_4$/ C	$LiPF_6$	Sol-gel method	Specific capacity – 140 mAhg^{-1} at 1C	**[21]**
Boqiao li et.al.,(2019)	$LiFePO_4$/ C	$LiNO_3$	Surfactant assisted hydrothermal method	Specific capacity – 163.2 mAhg^{-1} at 0.1C for 500 cycles	**[22]**
Sourav khan et.al.,(2019)	$LiFePO_4$/ C	LiOH	Surfactant assisted hydrothermal method	Specific capacity – 140 mAhg^{-1} at 0.1C for 100 cycles	**[23]**
FuAnGuo et.al., (2019)	$LiFePO_4$/ C	LiOH	Spray –drying process	Specific capacity-165mAhg^{-1}	**[24]**
Xiaoling cui et.al.,(2019)	$LiFePO_4$/ C-P	Li $_2CO_3$	Solid state reaction method	Specific capacity-82.7mAhg^{-1} at 0.1C	**[25]**
Huan Liu et.al., (2019)	$LiFePO_4$/ C	Li_2CO_3	Solid state reaction	Specific capacity-164.1 mAh g^{-1} at 0.1 C for 500 cycles	**[26]**
Virendra Patil et.al., (2019)	$LiFePO_4$	Li_2MO_3	Solvothermal reaction	Specific capacity-162 mAh g^{-1} at 0.1 C	**[27]**

W.Honggo wiranto et.al., (2019)	$LiFePO_4$	LiOH	Hydrothermal method	Specific capacity- 106.84 mAh g^{-1} at 0.1C	**[28]**
Junjie Lu et.al., (2019)	$LiFePO_4$	Li_2PO_4	Solvothermal method	Specific capacity- 101.4 mAh g^{-1} at 1C for 500 cycles	**[29]**
Hari Raja et.al., (2018)	$LiFePO_4$	$Li(CH_3COO) . 2H_2O$	Sol-gel method	Discharge capacity- 138 mAh g^{-1} for 200 cycles at 0.1 C	**[30]**
Lei Chen et.al., (2018)	$LiFePO_4$	LiOH	Spray-drying method	Specific capacity-162 mAh g^{-1} at 0.2 C for 50 cycles	**[31]**
Swapnil J. Rajaba et.al., (2018)	$LiFePO_4$	$LiNO_3$	Solution combustion method	Specific capacity-106 mAh g^{-1} Discharge capacity-164 mAh g^{-1} at 0.1C	**[32]**
Chuanli Qin et.al., (2017)	$LiFePO_4$/ Ethylene Glycol (EG)	LiH_2PO_4	Hydrothermal method	Specific capacity-170 mAh g^{-1}	**[33]**
Bo Wanga et.al., (2017)	$LiFePO_4$	LiOH	Thermal reduction method	Specific capacity-135 mAh g^{-1} at 0.3 C	**[34]**
S.J. Rajoba et.al., (2017)	$LiFePO_4$	Li_3PO_4	Solution combustion method	DC Conductivity-1.21 x 10^{-3} S/cm	**[35]**
Yaochum Yao et.al., (2016)	$LiFePO_4$/ C	Li_2CO_3	Solid state reaction	Specific capacity-87.6 mAh g^{-1} at 10C for 80 cycles	**[36]**
Alexis B., et.al., (2016)	$LiFePO_4$	LiH_2PO_4	Sol-gel method	Cyclic voltammetry was carried out at 1.0 mV/s between 2.0and 4.0V	**[37]**

Yawen Li et.al., (2016)	$LiFePO_4$/ Ethylene Glycol (EG)	$LiNO_3$	Sol-gel method	Current density 200 mAh g^{-1} for 100 cycles	**[38]**
Jinsub Lim et.al., (2015)	$LiFePO_4$/ GN (graphene nanosheets)	$Li(CH_3COO)$	Microwave assisted polyol method	Discharge capacity-108 mAh g^{-1}at 32 C.	**[39]**
Zhe-sheng feng et.al., (2015)	$LiFePO_4$/ cu	Li_2CO_3	Two step chemical process	Specific capacity -146.7 mAh g^{-1} at 0.1 C.	**[40]**
Hossein Ghafarian-Zahmatkesh et.al., (2015)	$LiFePO_4$/ Ethylene Glycol/C (EG)	$LiOH.H_2O$	Hydrothermal method	Discharge capacity-166 mAh g^{-1}at 0.1 C for 100 cycles.	**[41]**
Wei Weia et.al., (2014)	$LiFePO_4$/ CNT (carbon nano tube)	$LiOH.H_2O$	Hydrothermal method	Discharge capacity-122 mAh g^{-1}at 20 C for 500 cycles.	**[42]**
Zhenxin Liu et.al., (2014)	$LiFePO_4$/ C	LiOH	Co precipitation method	Discharge capacity-125 mAh g^{-1}	**[43]**
Chien –Te Hsieh et.al., (2013)	$LiFePO_4$	Li_2CO_3	Hydrothermal method	Specific power densities 400 Wh/Kg	**[44]**
Yun-Hwa Hwang et.al., (2013)	$LiFePO_4$/ C	Li_2CO_3	Solid state reaction	Discharge capacity-135 mAh g^{-1}at 0.1C Potential range 2.5-4.5 V	**[45]**

Jeongbin lee et.al., (2013)	$LiFePO_4$	Li_2CO_3	Solid state reaction	Discharge rates of 0.1C, 0.5C, 1.0C and cut off voltage 2.5V	**[46]**
Gary M. Koenig et.al., (2013)	$LiFePO_4$	Li_2CO_3	Solid state reaction	Cycle rate 10 mA g^{-1}. The discharge cycle between 2.0 and 4.0 V.	**[47]**
Jae-Kwangkim et.al., (2013)	$LiFePO_4$	Li_2CO_3	Sol-gel method	Specific capacity-118.5 mAh g^{-1} at the 100^{th} cycle High tap density-1.8 g cm^{-1}	**[48]**

CHAPTER III

MATERIALS AND METHODS

3.1 Introduction

This chapter deals with the experimental techniques used in the preparation and characterization of lithium iron phosphate for lithium-ion battery. The effect of different synthesis procedure on the electrochemical performance have been studied. The experimental techniques employed to understand the properties of prepared material are as follows:

- X-ray Diffraction (XRD)
- Cyclic voltammetry (CV)

3.2. Synthesis Techniques

Synthesis of cathode material, Lithium Iron Phosphate (LFP) is prepared through various techniques available in wet chemical Process. Wet chemical methods are used for producing nano and ultra-dispersed inorganic powders from aqueous and non-aqueous solutions. Some of the synthesis techniques under this process are,

- Sol-Gel Process
- Co-Precipitation Process
- Hydrothermal Process
- Solid state reaction

3.2. Sol gel method

The sol–gel process is a method for producing solid materials from small molecules. This method is used for the fabrication of metal oxides. The process involves conversion of monomers into a colloidal solution (*sol*) that acts as the precursor for an integrated network (or gel) of either discrete particles or network polymers. Typical precursors are metal alkoxides. Sol-gel process is used to produce ceramic nanoparticles.

3.2.1. Synthesis of lithium iron phosphate by sol gel method

3.2.1.1. Experimental details

Preparation of lithium iron phosphate carried out by sol-gel process is given below:

3.2.1.2. Raw material used

1. Lithium nitrate ($LiNO_3$)
2. Ferrous oxalate ($FeC_2O_4.2H_2O$)
3. Ammonium dihydrogen phosphate ($NH_4H_2PO_4$)
4. Citric acid monohydrate ($C_6H_8O_7.H_2O$)

The Lithium Iron Phosphate (LFP) was prepared by the sol-gel process. $LiNO_3$(Lithium nitrate), $FeC_2O_4.2H_2O$ (Ferrous oxalate), $NH_4H_2PO_4$(Ammonium dihydrogen phosphate),and $C_6H_8O_7.H_2O$ (Citric acid) were taken as starting material. The molar ratio of 1:1:1:1. These materials is dissolved in water. Then ferrous oxalate and $LiNO_3$ is added in a beaker and stirred for 1 hour. Ammonium dihydrogen phosphate is stirred for 30 minutes in a separate beaker. Citric acid is kept in another beaker and stirred for 30 minutes. After 1 hour ammonium dihydrogen phosphate is added to $LiNO_3$ and $FeC_2O_4.2H_2O$ Solution. Now after 15 min acid is added gradually to this solution. Now the total mixture is stirred up to 30 min. The mixture temperature is raised to 150℃ in stirrer. After 4 hours of stirring, the gel is formed. Now the gel formed is kept in the water bath for 2 hours. After 2 hours, the gel gets transformed to dry powder. The dried powder is taken for grinding. The precursor is kept in a furnace and calcined at 700℃ for 2h and the LFP prepared by sol-gel method is named as LFP-SG.

The chemical reaction involved in the formation of lithium iron phosphate discussed below:

$$LiNO_3+FeC_2O_4.2H_2O+NH_4H_2PO_4+C_6H_8O_4.H_2O = LiFePO_4+NH_3+CO_2+H_2O$$

The preparation of LFP using Li_2CO_3 precursor was attempted using sol-gel, co-precipitation and hydrothermal method and the preparation was not successful, since, the expected yield of the sample was not reaped. And hence the sample prepared from different method lithium precursor in different methods viz. sol-gel, co-precipitation and hydrothermal method.

3.3. Co precipitation method

The simultaneous precipitation of a normally soluble component with a macro-component from the same solution by the formation of mixed crystals, by adsorption, occlusion or mechanical entrapment.

3.3.1. Synthesis of lithium iron phosphate by co-precipitation method

3.3.1.1. Experimental details

Preparation of lithium iron phosphate is carried out by the co- precipitation method and the method is given below:

3.3.1.2. Raw material used

1. Ferrous sulphate ($FeSO_4.7H_2O$)
2. Lithium nitrate($LiNO_3$)
3. Ammonium dihydrogen phosphate ($NH_4H_2PO_4$)

The olivine $LiFePO_4$cathode material synthesized by co-precipitation method. The stoichiometric amount of $FeSO_4.7H_2O$, $LiNO_3$ and $NH_4H_2PO_4$ were dissolved in deionized water under vigorous stirring, then appropriate amount of ammonium hydroxide was added drop-wise to the solution to adjust the pH in the range of 8-9. The formed precipitate was separated by centrifuge, washed several times and dried at 150 °C. Then the powders were calcined at 700℃ for 12h. Finally obtained material is named as LFP-CP.

3.4. Hydrothermal method

Hydrothermal synthesis is a unique method for crystallizing substances from high-temperature aqueous solutions at high vapour pressures; also termed “hydrothermal method." The term “hydrothermal” is of geologic origin.

Hydrothermal synthesis can be defined as a method of synthesis of single crystals that depends on the solubility of minerals in hot water under high pressure. The crystal growth is performed in an apparatus consisting of a steel pressure vessel called an autoclave in which a nutrient is supplied along with water. A temperature gradient is maintained between the opposite ends of the growth chamber. At the hotter end the nutrient solute dissolves, while at the cooler end it is deposited on a seed crystal, growing the desired crystal.

3.4.1. Synthesis of lithium iron phosphate by hydrothermal method

3.4.1.1. Experimental details

Preparation of lithium iron phosphate carried out by the hydrothermal method and the preparation procedure is given below:

3.4.1.2. Raw material used

1. Ferrous sulphate ($FeSO_4.7H_2O$)
2. Phosphoric acid (H_3PO_4)
3. Lithium hydroxide monohydrate ($LiOH.H_2O$)

$LiFePO_4$/carbon black (LFP/CB) composite was prepared via a hydrothermal route using $FeSO_4.7H_2O$, H_3PO_4, and $LiOH.H_2O$ with the molar ratio of 1:1:3. Firstly, a suspension of Carbon black (3 wt.% of the obtained LFP) was mixed with 0.3 M LiOH aqueous solution and then aqueous solution of 0.1 M H_3PO_4 and 0.1 M $FeSO_4.7H_2O$ was added to the suspension at vigorous agitation for 5 min. Subsequently, the resulting mixture was then quickly transferred into a 100 mL Teflon-lined stainless-steel autoclave. LFP is formed by the reaction:

$$3LiOH + H_3PO_4 + FeSO_4 \leftrightharpoons LiFePO_4 + Li_2SO_4 + 3\ H_2O$$

To minimize the possibility of oxidation of $Fe^{2+}$to Fe^{3+}, the solutions are kept in hydrothermal autoclave and maintained at 170 ℃ for 5 h. The precipitates were centrifuged, washed with de-ionized water and dried at 60℃ overnight. The obtained LFP composite is named as LFP-HT.

3.5. Solid state method

The solid-state reaction route involves chemical decomposition reactions, in which a mixture of solid reactants is heated to produce a new solid composition and gases. This method is commonly used for the production of complex oxides from simple oxides, carbonates, nitrates, hydroxides, oxalates, alkoxides, and other metal salts.

3.5.1. Synthesis of lithium iron phosphate by solid state reaction method

3.5.1.1. Experimental details

Preparation of lithium iron phosphate is carried out by the solid state reaction method and the method is given below:

3.5.1.2. Raw material used

1. Lithium carbonate (Li_2CO_3)
2. Ferrous oxalate ($FeC_2O_4.2H_2O$)
3. Ammonium dihydrogen phosphate ($NH_4H_2PO_4$)

The LFP were prepared in the solid-state reaction method. Li_2CO_3(Lithium nitrate), $FeC_2O_4.2H_2O$ (Ferrous oxalate), $NH_4H_2PO_4$(Ammonium dihydrogen phosphate), and carbon black (CB) were taken as starting material. The molar ratio of Li_2CO_3, $FeC_2O_4.2H_2O$, and $NH_4H_2PO_4$are [1:1:1]. The Li_2CO_3, $FeC_2O_4.2H_2O$, $NH_4H_2PO_4$ were mixed and grinded for 20 min. Then 10 wt% of carbon black is added to the mixture and ground well for 1 hour .Then the mixture is heated at 380℃ for 6h. After 6h, the mixture cooled down to room temperature. The mixture is finally calcined at 750℃ for 12 h and the final LFP composite is named as LFP-SSR. Samples prepared with carbon addition were oxidising and turned rust coloured. Hence, carbon encapsulated LFPs were prepared and succeeded.

3.3 Characterization Techniques

3.3.1 X-Ray Diffraction (XRD)

For electromagnetic radiation to be diffracted, the spacing in the grating should be of the same order as the wavelength. In crystals, the typical interatomic spacing ~ 2-3 Å for the suitable radiation of X-rays. Hence, X-rays can be used for the study of crystal structures, Neutrons and Electrons and are also used for diffraction studies from materials [49].

3.3.2 Principle

X-Ray Diffractometer works on the principle of diffraction. Diffraction occurs when light is scattered by a periodic array with long-range order, producing constructive interferences at specific angles. The most commonly used technique is the powder X-Ray Diffraction to elucidate the crystalline nature of materials. The scattering of X-rays from atoms produce a diffraction pattern that contains information about the atomic arrangement in crystal.

XRD is effectively used for the structural determination, phase analysis, detection of preferred orientation, and deduction of an order disorder phenomenon and also determination of crystallite size of the powder samples [50].

3.3.3 Working

Diffraction effects are observed when electromagnetic radiation impinges on periodic structures with geometrical variations on the length scale of the wavelength of the radiation. The interatomic distances in crystals and molecules amount to 0.15–0.4 nm which correspond in the electromagnetic spectrum with the wavelength of x-rays having photon

energies between 3 and 8 keV. Accordingly, phenomena like constructive and destructive interference should become observable when crystalline and molecular structures are exposed to x-rays [51].

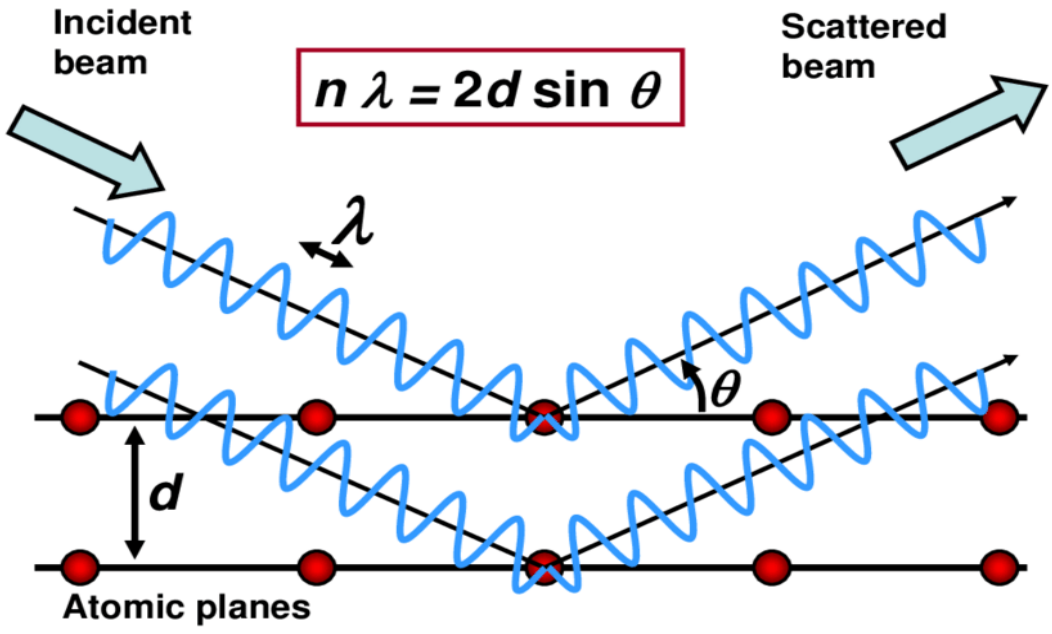

Figure 3.1. Schematic representation of X-ray production

Crystals are regular arrays of atoms, whilst X-rays can be considered as waves of electromagnetic radiation. Crystal atoms scatter incident X-rays, primarily through interaction with the atoms' electrons. This phenomenon is known as elastic scattering; the electron is known as the scatterer. A regular array of scatterers produces a regular array of spherical waves. In the majority of directions, these waves cancel each other out through destructive interference, however, they add constructively in a few specific directions, as determined by Bragg's law:

$$n\lambda=2d \sin\theta$$

- d is the spacing between atomic planes (Å)
- λ is the wavelength of X-rays (Å)
- θ is the diffraction angle (degrees)

3.3.4. Scherrer's Formula

If there is no homogeneous strain, the crystallite size (D), can be estimated from thepeak width with the Debye-Scherrer's formula,

$$D = k\lambda / \beta \cos\theta$$

- λ is the wavelength of X-rays (Å)
- β is the full width of half maximum (FWHM) of a diffraction peak (radians)
- θ is the diffraction angle (degree)
- k is the Scherrer's constant of the order of unity.

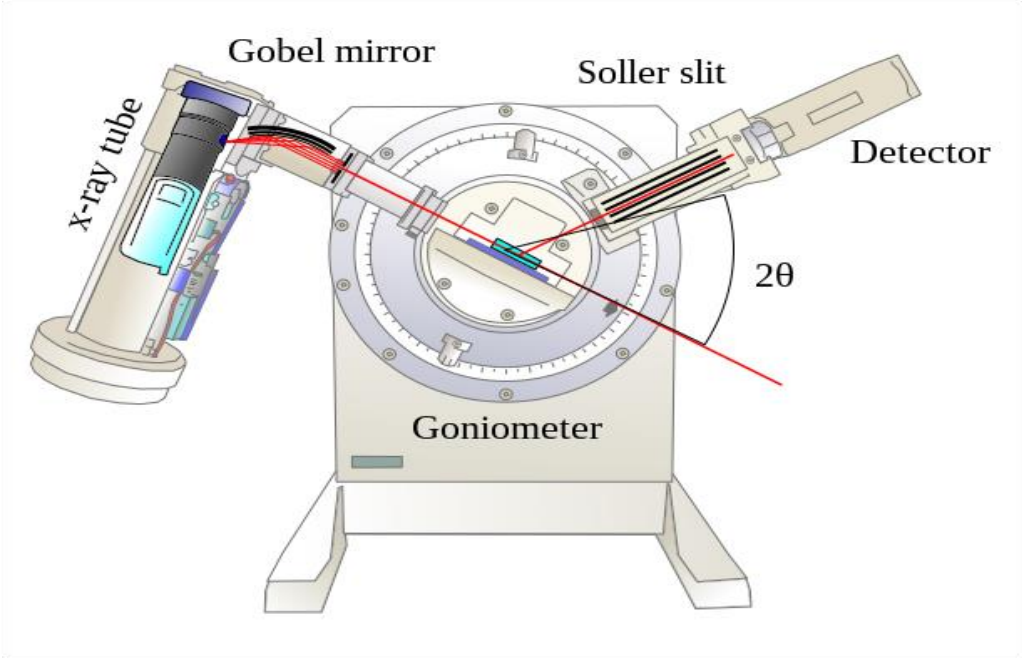

Figure 3.2 Powder X-Ray Diffractometer

The above Figure 3.2 shows the image of Powder X-Ray Diffractometer which is used for the analysis of various crystal structures [52].

3.4. Cyclic voltammetry

Cyclic voltammetry is an electrochemical technique used to measure the current response of a redox active solution to a linearly cycled potential sweep. It is a useful method

to find information about the thermodynamics of redox processes, the energy levels of the analyte and the kinetics of electronic-transfer reactions.

Like other types of voltammetry**,** cyclic voltammetry uses a three-electrode system consisting of a working electrode, a reference electrode, and a counter electrode.

To perform cyclic voltammetry, one need to start by adding your electrolyte solution to an electrochemical cell**,** along with a reference solution and the three electrodes. After this, use a potentiostat to linearly sweep the potential between the working and reference electrodes. When the potentiostat reaches the pre-set limit, it will sweep back in the opposite direction. The potentiostat will repeat this process multiple times during a scan. While doing so, it will record the changing current between the working and counter probes. The result is a characteristic duck-shaped plot known as a cyclic voltammogram [53].

3.4.1 Cyclic Voltammogram Explained

In this study, Biologic SP-150 is used to take the electrochemical measurements. A cyclic voltammogram is the 'duck-shaped' plot generated by cyclic voltammetry.

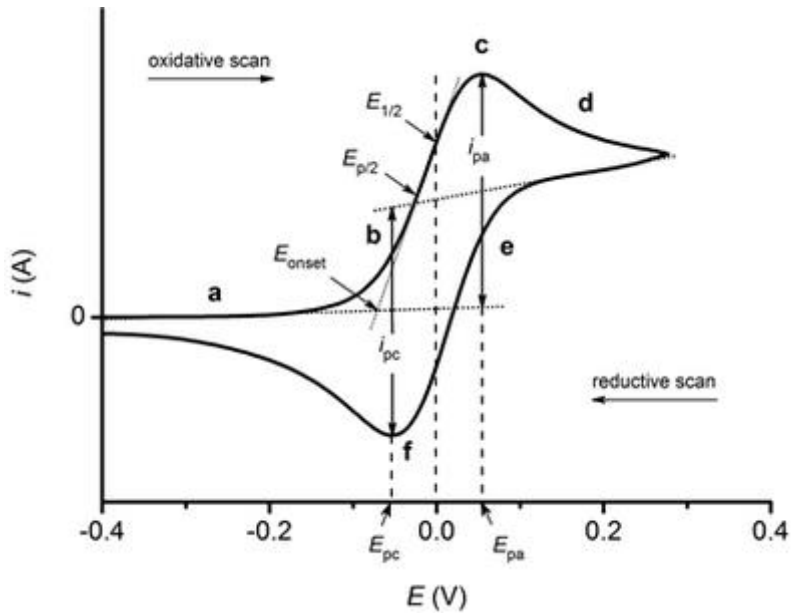

Figure 3.3 Cyclic voltammogram and analytics

Example of a cyclic voltammogram for an electrochemically reversible one-electron redox process. In the example cyclic voltammogram above, the scan starts at -0.4V and sweeps

forward to more positive, oxidative potentials. Initially the potential is not sufficient to oxidise the analyte.

As the potential approaches several of the standard potential, the onset (E_{onset}) of oxidation is reached. Following this, the current exponentially increases (b) as the analyte begins its oxidation at the working electrode surface. For a reversible process, here the current rises initially as if there is no change in the concentration of oxidant.

The current is dictated by the rate of diffusion of the oxidant to the electrode, as well as the proportion converted to the reduced form. This can be understood according to the Nernst equation. Gradually, as the scan continues, more oxidant is depleted. The concentration gradient adjusts to this. It is this change which causes a peak in the voltammogram. A decrease in current from depletion of the oxidant outweighs the increase from changing the proportion of oxidant oxidised at the electrode [54].

The current reaches peak maximum at point c (anodic peak current (i_{pa}) for oxidation at the anodic peak potential (E_{pa}). Here, more positive potentials cause an increase in current that is offset by a decreasing flux of analyte from further and further distance from the electrode surface.

From this point, the current is limited by the mass transport of analyte from the bulk to the interface, which is slow on the electrochemical timescale. This results in a decrease in current (d), as the potentials are scanned more positive. This occurs until a steady-state is reached where further increases in potential no longer has an effect.

Scan reversal to negative potentials (reductive scan) continues to oxidise the analyte. This continues until the applied potential reaches the value where the oxidised analyte (which has accumulated at the electrode surface) can be re-reduced (e).

The process for reduction mirrors that of the oxidation. The only difference is that it occurs with an opposite scan direction and a cathodic peak (i_{pc}) at the cathodic peak potential (E_{pc}) (f). The anodic and cathodic peak currents should be of equal magnitude but with opposite sign. This is the case only provided that the process is reversible and if the cathodic peak is measured relative to the base line after the anodic peak [55].

3.4.2 Applications

Cyclic voltammetry (CV) has become an important and widely used electroanalytical technique in many areas of chemistry. It is often used to study a variety of redox processes, to determine

the stability of reaction products, the presence of intermediates in redox reactions, electron transfer kinetics, and the reversibility of a reaction. It can be used for electrochemical deposition of thin films or for determining suitable reduction potential range of the ions present in electrolyte for electrochemical deposition. CV can also be used to determine the electron stoichiometry of a system, the diffusion coefficient of an analyte, and the formal reduction potential of an analyte, which can be used as an identification tool. In addition, because concentration is proportional to current in a reversible, Nernstian system, the concentration of an unknown solution can be determined by generating a calibration curve of current vs. concentration [56].

CHAPTER IV

RESULTS AND DISCUSSIONS

4.1 Introduction

This chapter deals with the analysis of Lithium iron phosphate prepared by four different methods viz., sol-gel method, solid-state reaction method, hydrothermal method and co-precipitation method. The structural and electrochemical behaviour of the prepared samples is compared and is discussed in this chapter.

The Lithium iron phosphate (LFP) prepared using sol-gel method, co-precipitation, hydrothermal method and solid-state reaction method are named as LFP-SG, LFP-CP, LFP-HT and LFP-SSR respectively.

4.2 Structural Characterization

4.2.1 X-ray diffraction (XRD) analysis of LFP prepared by sol gel method

The crystal structure of lithium iron phosphate (LFP) prepared by sol-gel method (LFP-SG) have been analysed by powder X-ray diffraction technique by using Bruker AXS D2 PHASER. Figure 4.1 depicts the XRD pattern of Lithium iron phosphate prepared by sol-gel method. All the diffraction peaks of lithium iron phosphate are compared to the JCPDS Card No. 81-1173 with orthorhombic structure of space group Pnma and lattice parameters a=10.33 Å, b=6.010 Å and c=4.692Å. The major diffraction peaks observed at 2θ=33.29°, 35.67° and 54.99° corresponding to hkl planes (220), (311) and (412) respectively. Other diffraction peaks observed nicely matches with the $LiFePO_4$ structure without any changes where the corresponding values of 2θ and hkl planes are indexed. The peaks observed at 2θ= 20.75°, 23.05°, 24.15°, 29.45°, 32.01°, 33.85°, 36.36°, 40.78°, 44.17°, 47.23°, 47.40°, 49.58°, 57.32°, 60.02°, 61.17°, 62.49°, 64.10°, 68.50°, 69.30°, 72.03°, 75.62° corresponding to miller planes indexed to (101), (210), (011), (211), (301), (400), (121), (401), (321), (230), (302), (022), (521), (013), (132), (620), (213), (531), (711), (413) and (142) respectively.

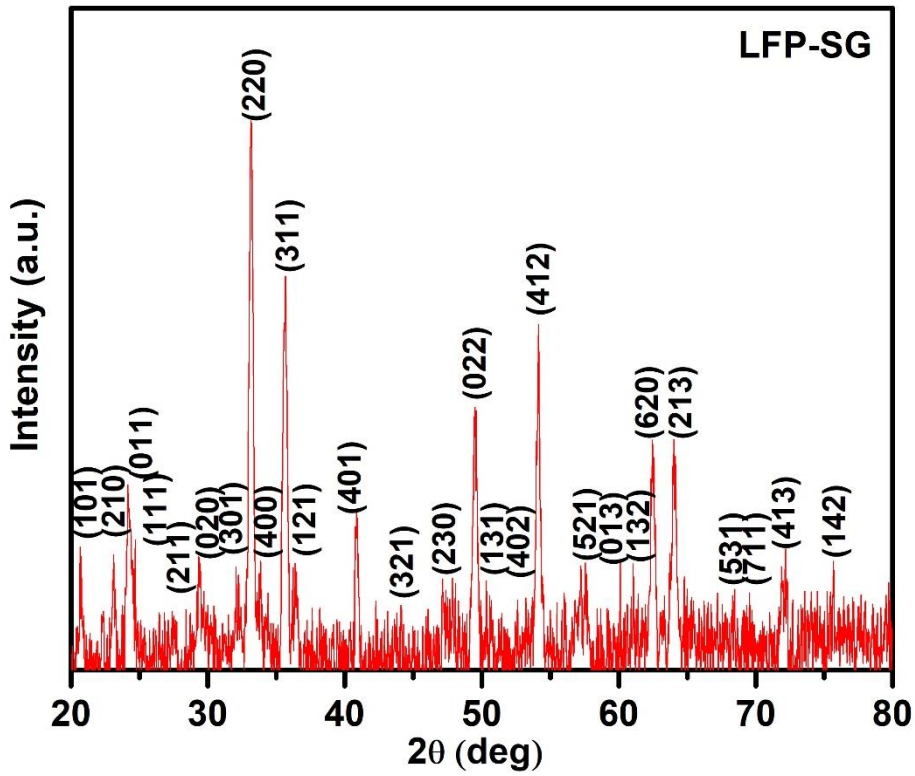

Figure 4.1 XRD pattern of lithium iron phosphate prepared by sol-gel method

The crystallite size of the as-prepared sample is calculated by using the Debye-Scherrer formula. The Debye Scherrer formula is

$$\mathbf{D} = \frac{k\lambda}{\beta cos\theta}\mathbf{(nm)}$$

where,

D is the crystallite size

k is Scherrer constant,

λ is the wavelength of the radiation (1.5405Å)

β is Full width half maximum of the peak.

The most prominent and highly intense peak at 33.29° corresponding to the plane (220) of LFP. The crystallite size is 16.61 nm calculated from the (220) plane. The observed peaks are sharp and intense which indicates the high crystallinity of the sample.

Table 4.1 Crystallite size of the major diffraction peak

Sample	2θ (deg)	β (FWHM) (deg)	Crystallite size D (nm)
LFP-SG	33.15	0.50	16.61

4.2.2. X-Ray Diffraction (XRD) analysis of LFP prepared by co-precipitation method

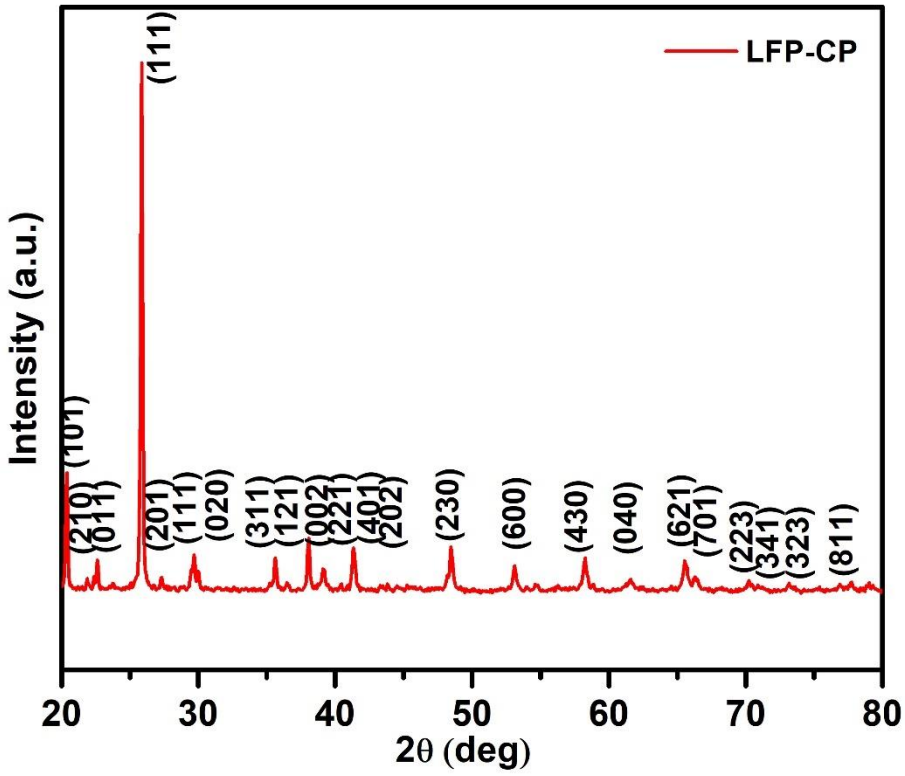

Figure 4.2 XRD pattern of $LiFePO_4$ prepared co-precipitation method (LFP-CP)

Figure 4.2 shows the XRD pattern of lithium iron phosphate (LFP) prepared, by co-precipitation method (LFP-CP) is shown in the Figure 4.2. All the diffraction peaks of lithium iron phosphate is compared to the JCPDS Card No.81-1173of $LiFePO_4$of orthorhombic structure. The major peak is observed at 2θ=25.70°, 20.35°, 38° corresponding to hkl planes (111), (101) and (002) respectively. Other diffraction peaks observed nicely matches with the

$LiFePO_4$ structure without any changes where the corresponding values of 2θ and hkl planes are indexed. The peaks observed at 2θ = 21.90°, 22.70°, 27.30°, 29.60°, 29.90°, 35.50°, 36.50°, 39.00°, 40.36°, 41.32°, 43.85°, 48.50°, 53.06°, 54.66°, 58.26°, 61.64°, 65.56°, 66.416°, 70.22°, 70.96°, 73.40°, 78.91° corresponding to miller planes indexed to (210), (011), (201), (211), (020), (311), (121), (221), (401), (112), (202), (230), (600), (412), (430), (040), (621), (701), (223), (341), (323) and (811) respectively. The observed peaks are sharp and intense which indicates the high crystallinity of the sample.

The most prominent and highly intense peak at 25.70° corresponds to the plane (111) of $LiFePO_4$ structure. The crystallite size is 12.84 nm for lithium iron phosphate (LFP-CP) calculated from (111) plane as shown in the Table 4.2.

Table 4.2 Crystallite size of the major diffraction peaks

Sample	2θ (deg)	β (FWHM) (deg)	Crystalline size D (nm)
LFP-CP	33.15	0.646	12.84

4.2.3. X-Ray Diffraction analysis of LFP prepared by hydrothermal method

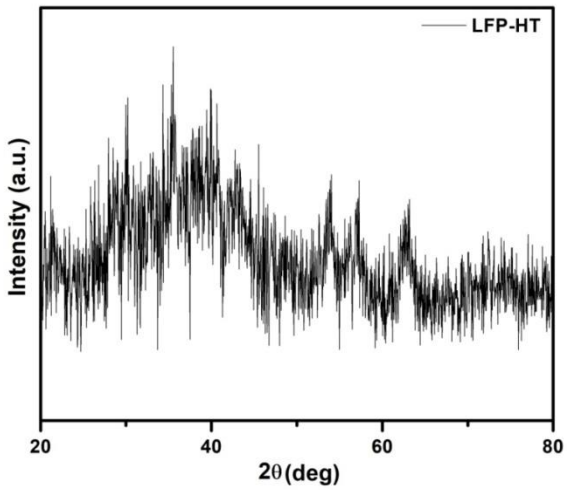

Figure 4.3 XRD pattern of LFP prepared by hydrothermal method

The sample prepared by hydrothermal method does not show refined diffraction peaks matched to $LiFePO_4$ phase which may be either due to the non-completion of reaction or

instrumental error. But few crystalline peaks are seen. The preparation may take more trials for confident neglection of this processing method.

4.2.4. X-Ray Diffraction (XRD) analysis of LFP prepared by solid-state reaction method

The crystal structure of lithium iron phosphate (LFP) prepared by solid state reaction method (LFP-SSR) is shown in the Figure 4.4. All the diffraction peaks of lithium iron phosphate is compared to the JCPDS Card No. #81-1173 of $LiFePO_4$of orthorhombic structure.

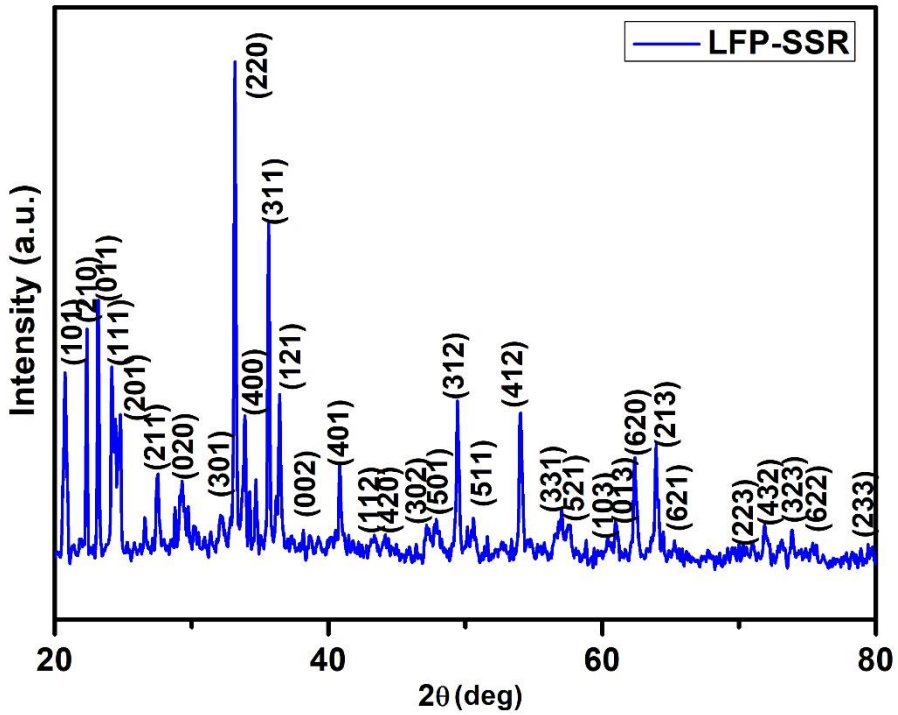

Figure 4.4 XRD pattern of $LiFePO_4$prepared by solid-state reaction method (LFP-SSR)

The major diffraction peaks are observed at $2\theta = 33.15^0$, 35.58^0, $23.13^0$with the corresponding miller planes (220), (311) and (011). The other diffraction peaks observed are listed in the Table 4.3. The diffraction peaks are well suited to the space group Pnma with lattice parameters a=10.33 Å, b=6.010 Å, c=4.693Å. The intensities of peaks differ due to the change in probable planes that is governed by the kinetics of growth which is very specific to the preparation method.

Table 4.3 Indexing planes for lithium iron phosphate prepared by Solid-state reaction method

No. of peaks	2θ (deg)	h	k	l
1	20.70	1	0	1
2	22.30	2	1	0
3	24.20	1	1	1
4	24.50	2	0	1
5	27.50	2	1	1
6	29.40	0	2	0
7	32.03	3	0	1
8	33.80	4	0	0
9	36.60	1	2	1
10	38.10	0	0	2
11	40.10	4	0	1
12	43.10	1	1	2
13	47.07	4	2	0
14	47.20	3	0	2
15	47.98	5	0	1
16	49.30	3	1	2
17	50.60	5	1	1
18	54.04	4	1	2
19	56.98	3	3	1
20	57.38	5	2	1
21	60.31	1	0	3
22	61.19	0	1	3
23	62.47	6	2	0
24	64.10	2	1	3
25	65.40	6	2	1
26	70.19	2	2	3
27	71.76	4	3	2
28	73.91	3	2	3
29	75.38	6	2	2
30	79.48	2	3	3

The most prominent and highly intense peak at 33.15^{0} corresponds to the plane (220) plane of LFP. The crystallite size is 20.93 nm for lithium iron phosphate calculated from (220) plane. The observed peaks are sharp and intense which indicates the high crystallinity of the sample.

Table 4.4 Crystallite size of the major diffraction peak

Sample Name	2θ (deg)	β (FWHM) (deg)	Crystalline size D (nm)
LFP-SSR	33.15	0.385	20.93

The XRD analysis of all the samples prepared by different methods are studied. The expected product $LiFePO_4$ is obtained in three cases of synthesis procedure of LFP. All the XRD pattern matches well with the JCPDS Card No. 81-1173 except the hydrothermal method. However, the XRD pattern observed for the sample prepared by solid state reaction method (LFP-SSR) shows a perfect match of the $LiFePO_4$ structure of the orthorhombic structure. Since, all the prepared samples have the same crystalline structure of orthorhombic, Pnma space group, the electrochemical performance is worth comparing. Since few of the peaks emerging faded in hydrothermal process also coincides, it is worth comparing that sample also to other samples.

4.3 Electrochemical analysis

4.3.1 Cyclic Voltammetry (CV) analysis of LFP by Sol-gel method

Cyclic Voltammetry (CV) analysis for the lithium ion phosphate is performed by electrochemical workstation (Biologic SP150). Cyclic voltammetry is used to determine the reversibility of a reaction, the diffusion coefficient of an analyte and the reduction potential of an analyte.

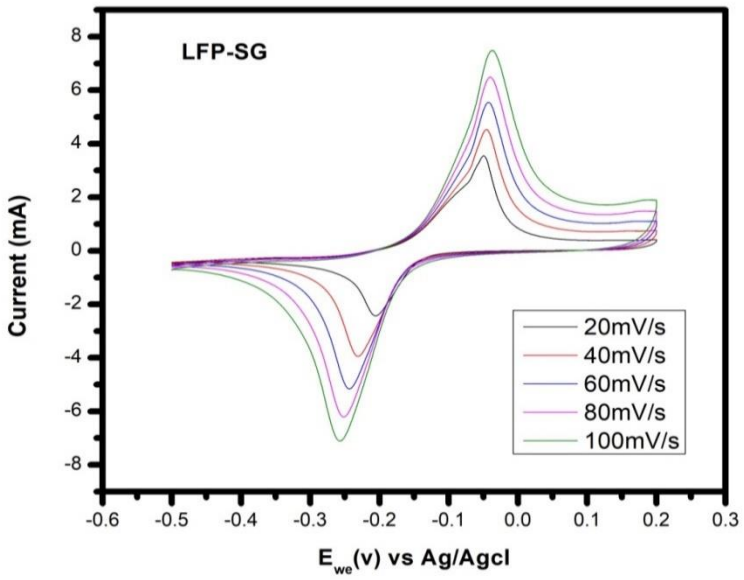

Figure 4.5 CV profile of LFP-1M LiOH

The diffusion coefficient of the electrochemical cells constructed using the as-prepared sample with LiOH electrolytes are given in the Table 4.6respectively.

The diffusion coefficient is calculated by using the formula,

where,

$$D = \left(\frac{B}{2.69\times10^{5}\ A\ Cn^{3/2}}\right)^{2}$$

B - Slope of the linear plot (mole/second)

A - Area of the electrode $(cm)^2$

C - Concentration of electrolyte (mole/litre)

Table 4.5 CV analysis of Lithium iron phosphate at electrolytic concentration of 1M-LiOH

Scan rate (mV/s)	**Potential (V)**		**Current (mA)**		**$\lvert E_{red}-E_{ox}\rvert$**	**$\lvert I_c / I_a \rvert$**	**Diffusion Coefficient cm^2s^{-1}**
	E_{ox}	**E_{red}**	**I_{ox}**	**I_{red}**			
20	-0.005	-0.20	3.13	-1.8	0.195	1.733	Anodic $0.439\times10^{-11}cm^2s^{-1}$
40	-0.004	-0.23	3.63	-3.23	0.226	1.123	

60	-0.041	-0.24	4.48	-4.28	0.199	1.046	Cathodic $0.4218x10^{-11}$ cm^2s^{-1}
80	-0.040	-0.25	4.82	-5.25	0.21	0.918	
100	-0.038	-0.25	5.43	-5.71	0.288	0.950	

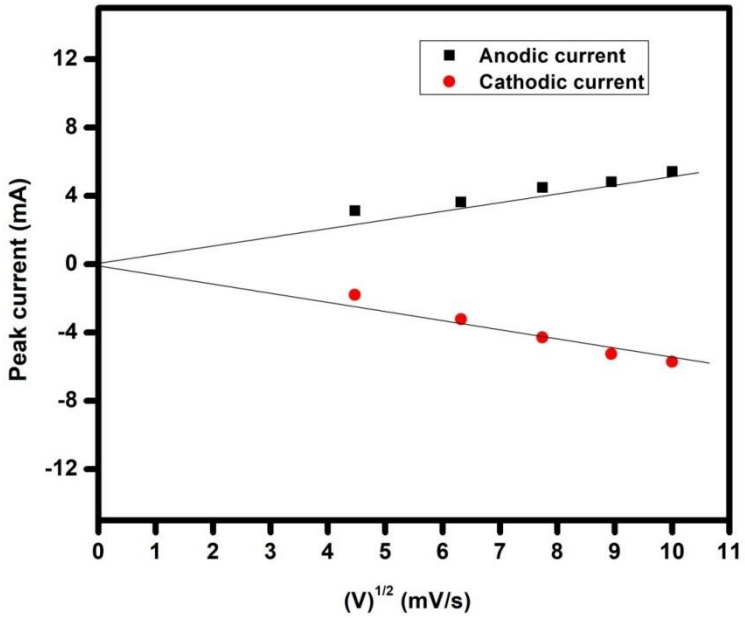

Figure 4.6 Plot of scan rate vs peak current for LFP- 1M LiOH

The prerequisites for a reversible electrochemical system (Nernstian system) are,

(i) Unity in peak current ratio,

(ii) Linearity between square root of scan rate and peak current,

(iii) Constant peak potential for different scan rates and

(iv) Peak separation more than or equal to 59 mV.

The peak current ratio of LFP-SG is nearly equal to 1, hence indicating a reversible nature of the system. A higher current value is obtained, which is nearly equal to 7mA for LFP-SG sample and the diffusion co-efficient calculated for both anodic and cathodic side are as $D_{anodic} = 0.439\times10^{-11}cm^2s^{-}1$ and $D_{cathodic} = 0.4218\times10^{-11}cm^2s^{-1}$.

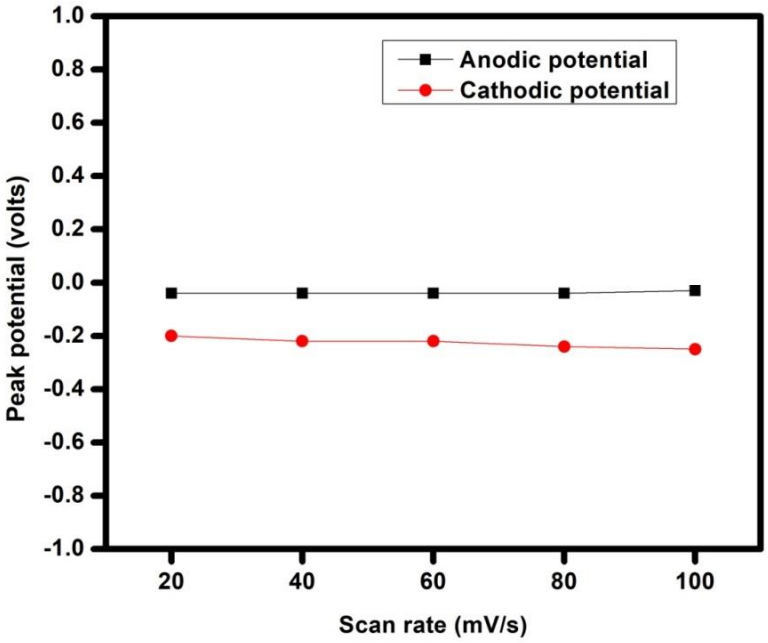

Figure 4.7 Plot of scan rate vs peak potential for LFP- 1M LiOH

Independency of peak potential with scan rate is observed from the CV graphs of the as-prepared sample in 1M LiOH electrolytic solution for different scan rates are shown in Figure 4.7.

4.3.2 Cyclic voltammetry (CV analysis) of LFP by co-precipitation method

Cyclic Voltammetry (CV) analysis for the lithium iron phosphate is performed by electrochemical workstation (Biologic SP-150). Cyclic voltammetry is used to determine the reversibility of a reaction, the diffusion coefficient of an analyte and the reduction potential of an analyte.

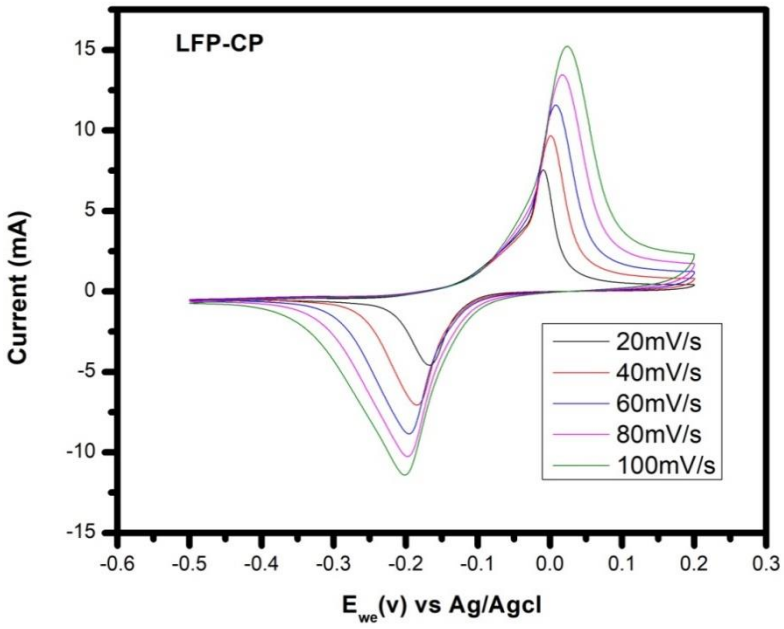

Figure 4.8 CV profile of LFP-1M Li-OH

Table 4.6 CV analysis of Lithium iron phosphate at electrolytic concentration of 1M-LiOH

Scan rate (mV/s)	Potential (V)		Current (mA)		$\lvert E_{red}-E_{ox}\rvert$	$\lvert I_c / I_a \rvert$	Diffusion Coefficient cm^2s^{-1}
	E_{ox}	E_{red}	I_{ox}	I_{red}			
20	-0.009	-0.16	6.78	-3.88	0.151	1.74	Anodic $2.322 \times 10^{-11} cm^2s^{-1}$
40	-0.003	-0.18	8.22	-6.15	0.177	1.33	
60	-0.007	-0.19	10.33	-8.06	0.183	1.28	Cathodic $1.384 \times 10^{-11} cm^2s^{-1}$
80	-0.01	-0.19	11.11	-9.18	-0.18	1.21	
100	-0.02	-0.20	12.72	-9.97	0.18	1.27	

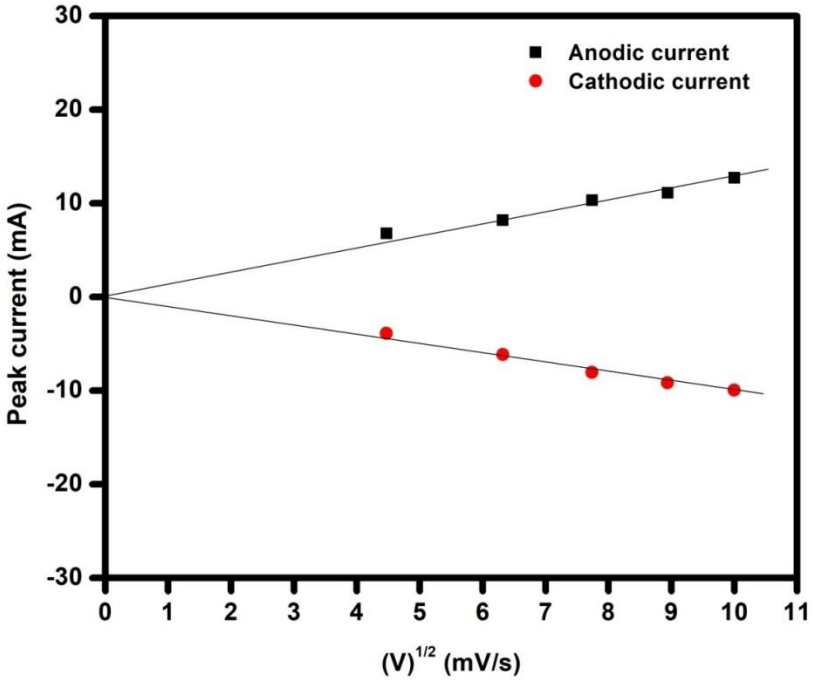

Figure 4.9 Plot of scan rate vs peak current for LFP- 1M LiOH

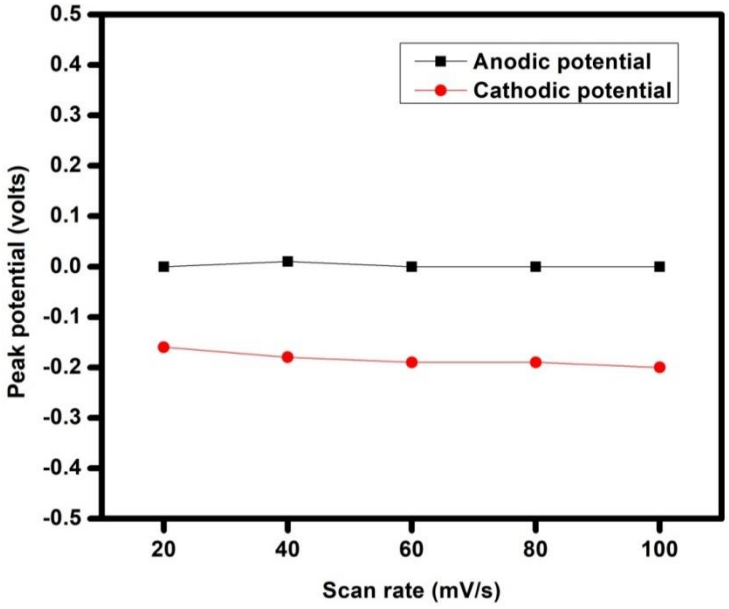

Figure 4.10 Plot of scan rate vs peak potential for LFP- 1M LiOH

Independency of peak potential with scan rate is observed from the CV graphs of the as-prepared sample in 1M LiOH electrolytic solution for different scan rates are shown in

Figure 4.9 and 4.10 respectively. From the above mentioned preparation it is clear that, maximum current of 15mA is obtained in co-precipitation method compared to sol-gel method.

4.3.3 Cyclic Voltammetry (CV) for LFP by solid state reaction method

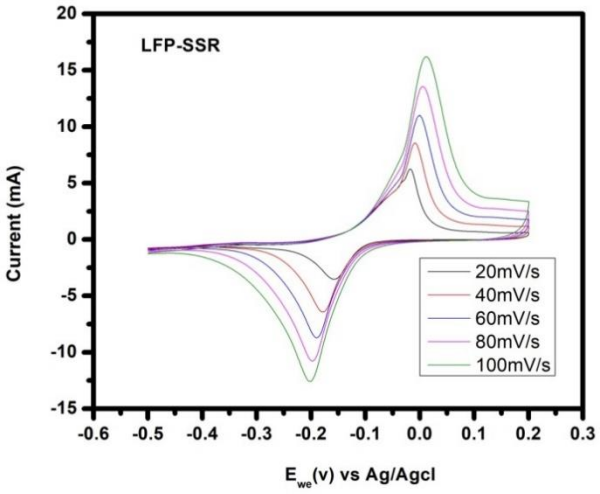

Figure 4.11 CV profile of LFP-1M Li-OH

Table 4.7 CV analysis of Lithium iron phosphate at electrolytic concentration of 1M-LiOH

Scan rate (mV/s)	Potential (V)		Current (mA)		$\|E_{red}-E_{ox}\|$	$\|I_c/I_a\|$	Diffusion Coefficient cm^2s^{-1}
	E_{ox}	E_{red}	I_{ox}	I_{red}			
20	-0.01	-0.15	5.35	-2.50	0.14	2.14	Anodic 1.925×10^{-11}
40	-0.009	-0.18	6.95	-5.08	0.17	1.36	
60	-0.001	-0.18	8.42	-7.12	0.17	1.18	Cathodic 1.384×10^{-11}
80	-0.004	-0.19	10.74	-9.45	0.18	1.13	
100	-0.01	-0.20	12.48	-11.47	0.18	1.08	

Also, linear increment between peak current and the square root of the scan rate of the LFP in 1M of LiOH are observed and are shown in Figure 4.12 and 4.13. In both the cases, not

all the peak currents are incremented linearly with respect to the square root of the scan rate there are some peak currents which fall under linear plot and they are within the error limits. The peak potentials are maintained constant during the CV profiling indicating the stability of the cell thus the working electrode.

The diffusion co-efficient of anodic and cathodic potentials are $1.925 \times 10^{-11}$and 1.384×10^{-11}S/cm which is comparatively lower than the sample prepared by sol-gel method. Hence, LFP prepared by solid-state reaction method shows good cycling performance and electrochemical activity satisfying the Nernstian condition since a pure phase has been confirmed by XRD analysis.

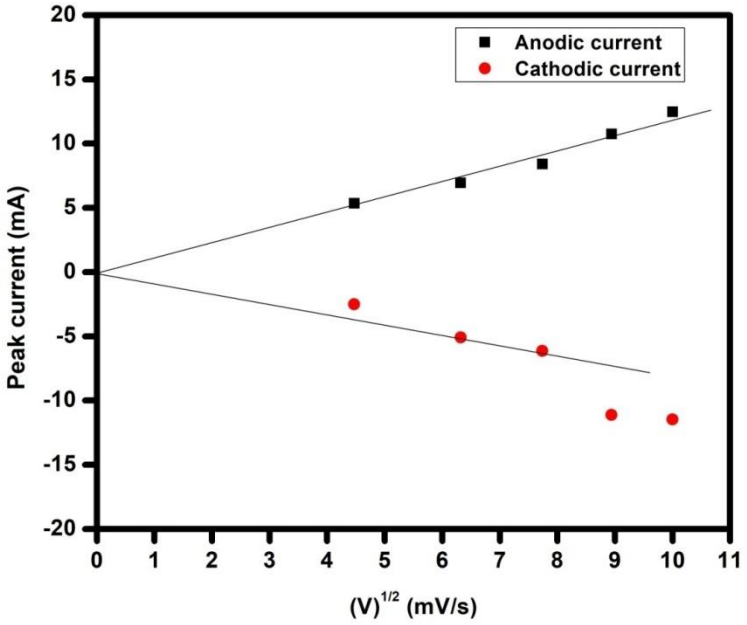

Figure 4.12 Plot of scan rate vs peak current for LFP- 1M LiOH

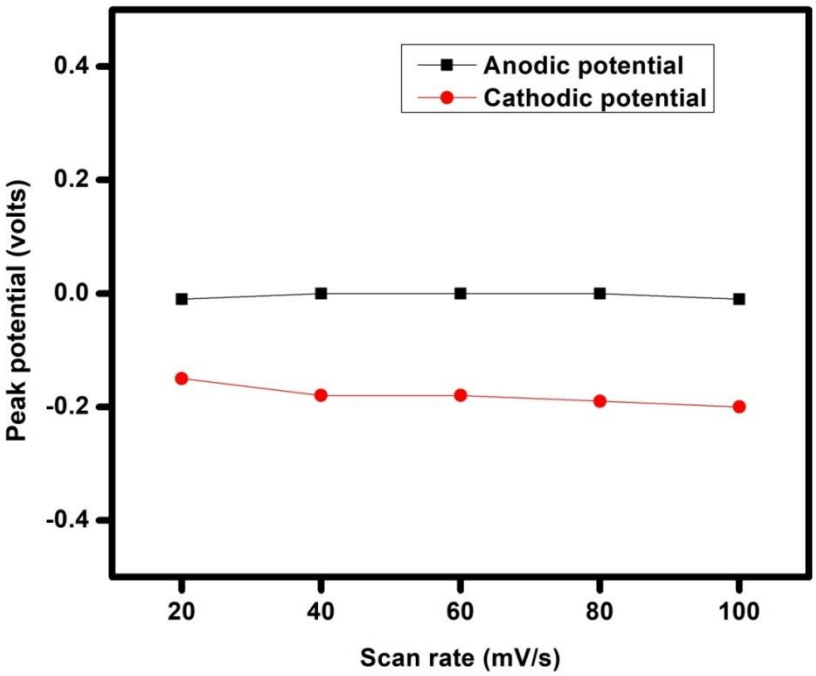

Figure 4.13 Plot of scan rate vs peak potential for LFP- 1M LiOH

Independency of peak potential with scan rate is observed from the CV graphs of the as-prepared sample in 1M LiOH electrolytic solution for different scan rates are shown in Figure 4.12 and 4.13 respectively.

Reviewing all the above performances, it clearly indicates that the chosen electrochemical system for LFP in 1M of LiOH electrolytic solution irrespective of preparation method exhibits slight deviation from the standard reversible nature, which can be ascribed as the quasi reversibility of the system.

The diffusion co-efficient obtained is higher for the solid-state reaction method. The D_{anodic} observed for the LFP-SSR is $1.925\times10^{-11}cm^2s^{-1}$ and $D_{cathodic}$ is $0.4218\times10^{-11}\ cm^2s^{-1}$.

Lithium carbonate is a cheaper salt available in the market and solid-state reaction method is a very low cost and easily scalable method of preparation for commercial or industrial purpose. The objective of preparing LFP from carbonate source is accomplished and the diffusion coefficient and stability are found to be better than the other preparation from nitrate and hydroxyl sources and other methods of preparation.

CHAPTER V

SUMMARY AND CONCLUSION

Lithium iron phosphate is prepared by four methods which is sol gel method (LFP-SG), co- precipitation method (LFP-CP), hydrothermal (LFP-HT) method and solid-state reaction method (LFP-SSR). The objective of the work is to prepare Lithium iron phosphate using low cost lithium precursor (Li_2CO_3) by any method of preparation. The prepared samples (LFP-SG, LFP-CP, and LFP-SSR) are well matched with the orthorhombic structure of $LiFePO_4$ sample except LFP-HT. The crystallite size of the samples are calculated using Debye-Scherrer formula. The crystallite size of lithium iron phosphate by sol gel method is 16.61 nm. The diffraction peaks observed for the LFP prepared by solid-state reaction method shows highly intense and sharp peaks which perfectly matches with the $LiFePO_4$ structure. The crystallite size of lithium iron phosphate by co precipitation method and solid state reaction method are 12.84 nm and 20.93 nm respectively. The samples are subjected to cyclic voltammetric analysis with 1M LiOH as an electrolyte. All the electrochemical performance of samples except LFP-HT are compared with each other since all the diffraction pattern lie in the same crystalline orthorhombic structure of Pnma space group. The Nernstian conditions are satisfied by all the samples. LFP prepared from solid-state reaction method accomplishes the objective of preparing LFP from Lithium carbonate source since it exhibits a higher degree of crystallinity, good stability and higher diffusion co-efficient than the samples prepared by nitrate, hydroxyl sources and other methods of preparation.

REFERENCES

[1] Yuqing Chen, Yuqiong Kang, Yun Zhao, Li Wang, Jilei Liu, Yanxi Li, Zheng Liang, Xiangming He, Xing Li, Naser Tavajohi, Baohua Li, Journal of Energy Chemistry, doi:https://doi .org/10.1016/j.jechem.2020.10.017.

[2] D. H. Doughty, E. P. Roth, Electrochemical Society Interface. 21 (2012),X. Feng, D. Ren, X. He, M. Ouyang, Joule. 4 (2020) 743-770. Doi:org/10.1016/j.jenvman.2020.110500.

[3] B. Dunn, H. Kamath, J. M. Tarascon, Science. 334 (2011) 928-935. Y. Kang, Z. Liang, Y. Zhao, H. Xu, K. Qian, X. He, T. Li, J. Li, Sci. China Mater. 63 (2020) DOI: 10.1007/s40843-020-1327-8.

[4] Michael M. Thackeray, Christopher Wolverton and Eric D. Isaacs ,energy and environmental science, Electrical energy storage for transportation—approaching the limits of, and going beyond, lithium-ion batteries The Royal Society of Chemistry 2012,Doi:10.1039/C2EE21892E.

[5] https://smartgrid.ieee.org/images/files/pdf/battery,storage,whitepaper.pdf.

[6] https://www2.chem.wisc.edu/deptfiles/genchem/netorial/rottosen/tutorial/modules/electrochemistry/06battery/18.64.htm.

[7] https://robu.in/working-of-lithium-ion-battery.

[8] Mogalahalli V. Reddy , Alain Mauger , Christian M. Julien , Andrea Paolella and Karim Zaghi, Brief History of Early Lithium-Battery Development, Materials 2020, 13, 1884; doi:10.3390/ma13081884.

[9] https://etn.news/energy-storage/cathode-the-energy-source-of-a-li-ion-battery.,

[10] Recent development and future prospects for lithium rechargeable batteries. Journal of power Sources, Vol.96, (June 2001), DOI:ISSN 0378-7753.

[11] Jiangtao Hu , Weiyuan Huang , Luyi Yanga and Feng Pan, Structure and Performance of $LiFePO_4$ Cathode Material: from Bulk to Surface, DOI:org/10.1039/D0NR03776A.

[12] Carlos A. G. Bezerra, Roge´ rio A. Davoglio, Sonia R. Biaggio, Nerilso Bocchi, and Romeu C. Rocha-Filho, “High-purity LiFePO4 prepared by a rapid one-step microwave-assisted hydrothermal synthesis”, J Mater Sci, 56:1001810029, 2021, doi:10.1007/s -021-05914-1.

[13] Yin Li, Li Wang, Keyu Zhang, Yaochun Yao, Lingxin Kong, “Optimized synthesis of LiFePO4 cathode material and reaction mechanism during

solvothermal", Advanced Powder Technology, vol.32, 2097–2105, 2021, doi:10.1016/j.apt.2021.04.019.

[14] Chaironi Latif, Anisa Fitri Muyasaroh, Amalia Firdausi, Dina Mardiana Wantana Klysubun, Chatree Saiyasombat, Bambang Prihandoko, Mochamad Zainuri Suminar Pratapa, "Preparation and characterization of $LiFePO_4$ ceramic powders via dissolution method", Ceramics International, Vol.47 (22), 31877 to 31885, 2021, doi: 10.1016/j.ceramint.2021.08.073.

[15] Yu-Xuan Bai, Jing Zhang, Yu-Bing Yang, Rong Yang, Ying-Lin Yan, Juan Wang, "Enhance electrochemical performance of LiFePO4 cathode material by Al-doped $Li_7La_3Zr_2O_{12}$ and carbon co-coating surface modification, Journal of Alloys and Compounds, Vol.843, 2020, doi:10.1016/j.jallcom.2020.154915.

[16] Wen-Chen Chien , Ya-Ru Li, She-Huang Wu, Yi-Shiuan Wu, Zong-Han Wu, Ying-Jeng James Li, Chun-Chen Yang, "Modifying the morphology and structure of graphene oxide provides high-performance $LiFePO_4$/C/rGO composite cathode materials", Advanced Powder Technology, Vol.31 (11), 4541-4551, 2020, doi:10.1016/j.apt.2020.10.002.

[17] Qianqian Li, Rengui Xiao, Xia Liao, Zhiming Ma, Yu Huang, Yunyan Zhang, Xiang Ke, "Extra Li-ion storage of $LiFePO_4$/C composite materials synthesized withFe1.5P", Journal of Alloys and Compounds, vol.835, 2020, doi:10.1016/j.jallcom.2020.155148.

[18] Xiaoning Tian, Weiheng Chen, Zhongqing Jiang, Zhong-Jie Jiang, "Porous carbon-coated LiFePO4 nanocrystals prepared by in situ plasma-assisted pyrolysis as superior cathode materials for lithium ion batteries", Ionics, Vol.26 (6), 2715 – 2726, doi:10.1007/s11581-019-03422-6.

[19] Bo Wang, Zekun Zhang, Yu Ning, Xinkui Li, Tingting Ruan, Fei Wang, Dianlong Wang,and Yu Zhou, "Construction of Dual-Carbon Co-Modified LiFePO4 Nanocrystals via Micro reactor Strategy for High Performance Lithium Ion Batteries", Energy Technol., 8, 2000171, 2020, doi: 10.1002/ente.202000171.

[20] Youngsu Kuk, Jieun Hwang, Dongho Nam, Jaehoon Kim, "Facile synthesis of high-performance LiFePO4-reduced graphene oxide composites using ball milling", Ionics, 2019, doi:10.1007/s11581-019-03395-6.

[21] Ju-Won Jeoa, Manik C. Biswas, Corey L. Pattonb, Evan K. Wujcik, "Water-processable, sprayable LiFePO4/graphene hybrid cathodes for high-power lithium ion batteries", Journal of Industrial and Engineering Chemistry, 84, 72–81, 2020, doi:10.1016/j.jiec.2019.12.022.

[22] Boqiao Li, Wei Zhao,Chen Zhang, Zhe Yang, Fei Dang, YiLun Liu, Feng Jin , and Xi Chen, “Monodispersed LiFePO4@C Core-Shell Nanoparticles Anchored on 3D Carbon Cloth for High-Rate Performance Binder-Free Lithium Ion Battery Cathode”, Journal of Nanomaterials, 2020, doi:10.1155/2020/2607017.

[23] Sourav Khan, Rayappan Pavul Raj, Laurel George,G. S. Kamali Kannangara, Adriyan Milev, Upadhyayula V. Varadaraju, and Parasuraman Selvam, “Surfactant-Mediated and Morphology- Controlled Nanostructured LiFePO4/Carbon Composite as a Promising Cathode Material for Li- Ion Batteries”, Chemistry Open , vol.9 (1), 23 – 31, 2019, doi:10.1002/open.201900175.

[24] FuAn Guo; Zhen Kong; Tao Wang; Xuehua Liu; Zheng Guan; Aiping Fung; Yanhui Li; Peizhi Guo; Yu-Guo Guo; Hongliang Li, “Porous microspheres consisting of carbon-modified LiFePO4 grains prepared by a spray drying assisted approach using cellulose as carbon source”, Ionics, 2019, doi:10 .1007/s11581-019-03388-5.

[25] Xiaoling Cui; Kuanyou Tuo; Yingchun Xie; Chunlei Li; Dongni Zhao; Li Yang; Xiaolan Fu; Shiyou Li, “Investigation on electrochemical performance at the low temperature of LFP/C-P composite based on phosphorus doping carbon network”, nanoscience and nanotechnology, 26, 3795–3808,2020, doi.10.1007/s11581-020-03567-9.

[26] Huan Liu, Shao-hua Luo, Sheng-xue Yan, Ya-feng Wang, QingWang, Ming-qi Li, Ya-hui Zhang, “A novel and low-cost iron source for synthesizing Cl-doped LiFePO4/C cathode materials for lithium-ion batteries”, Journal of Electroanalytical Chemistry, 850, 113434, 2019, doi.10.1016/j.jelechem.2019.113434.

[27] Youngsu Kuk, Jieun Hwang, Dongho Nam, Jaehoon Kim, “Facile synthesis of high-performance LiFePO4-reduced graphene oxide composites using ball milling”, Ionics, Vol.26 (6), 2803 – 2812, doi:10.1007/s11581-019-03395-6.

[28] Virendra Patil, Woong Oh, Jong Won Yoo, Lyongsun Pu, Jong Hyeok Park, Won-Sub Yoon, Gi-Ra Yi, “Carbon-Coated Supraballs of Randomly Packed LiFePO4 Nanoplates for High Rate and Stable Cycling of Li-Ion Batteries”, Particle and particle system characterization, Vol.36 (7), 2019, doi:10.1002/ppsc.201900149.

[29] W. Honggowiranto, E. Kartin, Sudaryanto, R. N. S. Rofika, E. Hutamaningtyas, A. Subhan, A. Sudjatno, “Improving Performance of LiFePO4 by addition of Carbon Nano Tube for Lithium Ion Battery”, IOP Conference Series: Materials Science and Engineering, Vol.553 (112), 2019, doi:10.1088/1757-899X/553/1/012060.

[30] Junjie Lu, Wenlong Li, Chao Shen, Dongmei Tang, Lanxuan Dai, Guowang Diao, Ming Chen, "Nano-scale hollow structure carbon-coated LiFePO4 as cathode material for lithium ion battery", Ionic ,Vol.25 (9), 407 – 408, doi:10.1007/s11581- 019-02978-7.

[31] Hari Raja, Sonia Ranib and Anjan Sila, "Antisite defects in sol-gel synthesized LiFePO4 at higher temperature: the effect on lithium ion diffusion", vol.5 (22), November 13, 3525-3532, 2018, doi:10.1002/celc.201800889.

[32] Lei Chen, Zhenyu Chen, Shuaishuai Liu, Haitao Zhang, and Quanzhen Huang, "Study on Highly Compacted LiFePO4/C Cathode Materials for High-performance 18650 Li-ion Batteries", Int. J. Electrochem. Sci., 13, 5413 – 5424, 2018, doi: 10.20964/2018.06.21.

[33] Swapnil J. Rajoba, Lata D. Jadhav, Ramchandra S. Kalubarme, Sanket N. Yadav, "Influence of synthesis parameters on the physicochemical and electrochemical properties of LiFePO4 for Li-ion battery", Journal of Alloys and Compounds, 2018, doi:10.1016/j.jallcom.2018.09.325.

[34] Chuanli Qin, Yawen Li, Shixian Lv, Junyu Xiang, Chenlong Wang, Xugang Zhang, Shen Qiu, Gleb Yushin, "Enhancing electrochemical performance of LiFePO4 by vacuum-infiltration into expanded graphite for aqueous Li-ion capacitors", Electrochimica Acta Vol.253, 413 – 421, 2017, doi:10.1016/j.electacta.2017.09.069.

[35] Bo Wang, Ying Xie, Tong Liu, Hao Luo, Bin Wang, Chunhui Wang, Lei Wang, Dianlong Wang, Shixue Doue, Yu Zhou, "$LiFePO_4$ quantum-dots composite synthesized by a general micro reactor strategy for ultra-high-rate lithium ion batteries", Nano energy,

[36] S.J. Rajoba, D. Jadhav, P.S. Patil, D.K. Tyagi, S. Varma, B.N. Wani, "Enhancement of Electrical Conductivity of LiFePO4 by Controlled Solution Combustion Synthesis", Journal of electronic materials, Vol.6 (3), 1683 –1691, doi:10.1007/s11664-016-5212-z.

[37] Yaochun Yao, Pengwei Qu, Xiangkun Gan, Xiaopeng Huang, Quanfeng Zhao, Feng Liang, "Preparation of porous-structured LiFePO4/C composite by vacuum sintering for lithium-ion battery", Ceramics International, Vol.42 (16), 17947-19466, 2016, doi.10.1016/j.ceramint.2016.08.158.

[38] Alexis B., Cyril Faur, Manuel Röder, Pierre Hovington, Uwe Posse, Abdelbast Guerfi Karim Zaghib, "Chemically fabricated LiFePO4 thin film electrode for transparent batteries and electrochromic devices", Materials Science and Engineering, 214, 81–86, 2016, doi:10.1016/j.mseb.2016.10.001 .

[39] Yawen Li, Dan Fu, Xugang Zhang, Shen Qiu1, Chuanli Qin, "Preparation, morphology and electrochemical performances of LiFePO4-expanded graphite composites as the

positive material for Li-ion capacitor application in aqueous neutral electrolyte", Journal of material science, Vol.27 (5), 4417 – 4425, doi:10.1007/s10854-016-4312-0.

[40] Jinsub Lim, Jihyeon Gim, Jinju Song, Dang Thanh Nguyen, Sungjin Kim, Jeonggeun Jo, Vinod Mathew, Jaekook Kim, "Direct formation of LiFePO4/graphene composite via micro wave assisted polyol process", Journal of power source, Vol.304, 354 – 359, 2015, doi:10.1016/j.jpowsour.2015.11.069.

[41] Zhe-sheng Feng, Lu-lin Wang, Yan Wang, Jin-ju Chen, Zhen-yu He, Ding-yu Ji, Yi-Xuan Zhang, "Improved electrochemical properties of LiFePO4/Cu cathode material synthesized via an optimized two-step chemical process", Journal of Alloys and Compounds, 651, 2015, DOI:10.1016/j.jallcom.2015.08.166.

[42] Hossein Ghafarian-Zahmatkesh, Mehran Javanbakht, Mehdi Ghaemi, "Ethylene glycol- assisted hydrothermal synthesis and characterization of bow-tie-like lithium iron phosphate nanocrystals for lithium-ion batteries", Journal of Power Sources, Vol.284, 339-348, 2015, doi:10.1016/j.jpowsour.2015.02.157.

[43] Sung Hoon Ha and Yun Jung Lee, "Core–Shell LiFePO4/Carbon-Coated Reduced Graphene Oxide Hybrids for High-Power Lithium-Ion Battery Cathodes", A European Journal, Vol.21, 5, 2132 – 2138, 2014, doi:10.1002/chem.201404952.

[44] Wei Weia, Linlin Guoa, Xiaoyang Qiua, Peng Qua, Maotian Xua, Lin Guo, "Porous Micro- spherical LiFePO4/CNT Nanocomposite for High Performance Li Ion Battery Cathode Material", RSC advance, Vol.5 (47), 37830 – 37836, doi:10.1039/c5ra05988g.

[45] Zhenxin Liu, Jingjing Li, Yu Xing, Lizhen Wang, Shaoming Fang, Bei Xu, Xiongwei Qu, "LiFePO4/C composites derived from precipitated FePO4 precursor: effects of mixing processes", Ionics 20, 1511–1516, 2014, doi: 10.1007/s11581-014-1110-7.

[46] Chien-Te Hsieh, Chun-Ting Pai, Yu-Fu Chen, I-Ling Chen, Wei-Yu Chen, "Preparation of lithium iron phosphate cathode materials with different carbon contents using glucose additive for Li-ion batteries", Journal of the Taiwan Institute of Chemical Engineers, Vol.45 (4), 1501 – 1508, 2013, doi:10.1016/j.jtice.2013.12.017.

[47] Yun-Hwa Hwang, S. J. Richard Prabakar, and Myoungho Pyo, "C-LFP-Multi-Walled Carbon Nanotubes Composite Cathode Materials Synthesized by Solid-State Reaction for Lithium Ion Batteries", Journal of Nanoscience and Nanotechnology, Vol.13, 5440–5444, 2013, doi:10.1166/jnn.2013.7036.

[48] Jeongbin Lee, Jaeshin Yi, Chee Burm Shin, Seung Ho Yu, Won Cho, "Modeling the Effects of the Cathode Composition of a Lithium Iron Phosphate Battery on the Discharge Behavior", Energies, 6, 5597-5608, 2013, doi:10.3390/en6115597.

[49] https://www.iitk.ac.in/che/pdf/resources/XRD-reading-material.pdf

[50] X-ray Diffraction @ McGill http://eps. mcgill. ca/xrd/howxrdworks. html. accessed May 3, 2023.

[51] BraggsLaw https://serc. carleton. edu/msu_nanote BraggsLaw. html.[accessed May 3, 2023.

[52] Sevćik, A. Collection of Czechoslovak Chemical Communications 1958, 13, 349.

[53] A. L. Bard and L. Faulkner Electrochemical methods: Fundamentals and Applications, 2nd ed. John Wiley & Sons 2001.

[54] W. L. G. Armarego and C. L. L. Chai Purification of Laboratory Chemicals, 7th ed. Butterworth-Heinemann 2012.

[55] L. J, L. B, and P. G Advanced Practical Organic Chemistry, 3rd edition. Manipal: Routledge 2013.

[56] J. L. Brédas, R. Silbey, D. S. Boudreaux, and R. R. Chance Chain-Length Dependence of Electronic and Electrochemical Properties of Conjugated Systems: Polyacetylene, Polyphenylene, Polythiophene, and Polypyrrole J. Am. Chem. Soc., vol. 105, no. 22, pp. 6555–6559, 1983.